ABSTRACT

Title of thesis: BALLISTOCARDIOGRAM-BASED APPROACH TO UBIQUITOUS BLOOD PRESSURE MONITORING

Stephanie Lind-Ober Martin, Master of Science, 2017

Thesis directed by: Associate Professor Jin-Oh Hahn
Department of Mechanical Engineering

Hypertension is a large contributor to cardiovascular deaths in the United States and around the world. Despite this fact, lack of ubiquitous blood pressure monitoring remains a large gap in modern-day health care. This thesis shall present a ballistocardiogram-based approach to ubiquitous blood pressure monitoring. Two approaches are presented: a signal-based approach and a model-based approach. The signal-based approach validates the superiority of ballistocardiogram-based pulse transit time as a reliable marker for BP over current electrocardiogram-based pulse arrival time methods. Concepts from the signal-based approach are then combined with a mechanism model of the ballistocardiogram and arterial hemodynamic modeling methods to produce a model-based approach. Two model-based variants are presented and the results of each are discussed. Despite certain limitations of the model-based approach, both variants are shown to still be more reliable than electrocardiogram-based pulse arrival time for blood pressure prediction. This work provides the foundation for a truly ubiquitous blood pressure monitoring method

and paves the way for early detection and continuous monitoring of cardiovascular health issues.

BALLISTOCARDIOGRAM-BASED APPROACH TO UBIQUITOUS BLOOD PRESSURE MONITORING

by

Stephanie Lind-Ober Martin

Thesis submitted to the Faculty of the Graduate School of the
University of Maryland, College Park in partial fulfillment
of the requirements for the degree of
Master of Science
2017

Advisory Committee:
Associate Professor Jin-Oh Hahn, Chair/Advisor
Professor Balakumar Balachandran
Professor Shapour Azarm

Dedication

To my loving husband Joshua. You have been a constant source of encouragement and stability throughout this work. I dedicate this thesis to you as a lasting sign of my appreciation and love for you.

Acknowledgments

I owe my gratitude to my adviser, Dr. Jin-Oh Hahn, for his support and direction throughout this thesis. I also wish to acknowledge the other members of my thesis committee of Dr. Balakumar Balachandran and Dr. Shapour Azarm for their support. I would also acknowledge Dr. Ramakrishna Mukkumala at the University of Michigan who directed the studies performed in this thesis.

I am also indebted to my parents, Dr. Curtis and Mrs. Virginia Ober. Without their hand in my education, from my mother educating me through high school to my father being a constant source of support in my collegiate career, I would not be where I am today. And to Andria Laib, for her support as a friend throughout this work. Your encouragement through laughter and tears has helped keep me grounded.

Finally, this research would not have been possible without the support of many sponsors. The sponsorship of the National Science Foundation (NSF) under Grant IIS 1404436 and the National Institutes of Health (NIH) under Grant EB-018818 where invaluable. I was also supported by the Dean's Fellowship Award given to me by the University of Maryland.

Contents

List of Tables

List of Figures

List of Abbreviations

BCG	-	Ballistocardiogram
BP	-	Blood Pressure
DBP	-	Diastolic Blood Pressure
ECG	-	Electrocardiogram
FPM	-	Full Parameter Model
HR	-	Heart Rate
ICG	-	Impedance Cardiography
PAT	-	Pulse Arrival Time
PEP	-	Pre-Ejection Period
PP	-	Pulse Pressure
PPG	-	Photoplethysmography
PTT	-	Pulse Transit Time
RMSE	-	Root-Mean-Square Error
RPM	-	Reduced Parameter Model
SBP	-	Systolic Blood Pressure

Chapter 1: Introduction

1.1 Background and Motivation

Blood pressure (BP) monitoring is key to ascertaining a persons current and long term health. A patient with high blood pressure (hypertension) is at increased risk of heart attacks, strokes, and kidney failure, among others. Hypertension has been called the "silent killer" since this condition does not cause discomfort and can easliy go undetected all while causing significant damage over time. Despite this fact, most patients receive only occasional, short-term blood pressure monitoring, either at the doctors office or a clinic (such as a local pharmacy). This approach does not elucidate real-time monitoring or identification of changes to the patients overall cardiovascular health. In stark contrast to this lack of care, a large proportion of deaths are due to cardiovascular issues. According to the CDC, there are over 600,000 deaths per year due to heart disease in the United States alone [2]. Of these deaths, 40.6% are due to high blood pressure [3]. Thus there is a clear need for ubiquitous (that is, non-invasive and continuous) blood pressure monitoring techniques to enable the prevention of deaths due to high blood pressure.

1.2 Current Blood Pressure Monitoring Techniques

A number of methods have been developed for BP monitoring which include auscultation, oscillometry, volume clamping, tonometry, and catheterization. Each method can be categorized as either invasive, manual, or cuff-based. A brief discussion of these techniques, and their shortcomings for ubiquitous BP monitoring is provided throughout the remainder of this section.

At the pinnacle of BP measurement techniques is catheterization. This method involves inserting a sensor, in the form of a small hollow tube, into the heart through the ascending aorta. While highly accurate, the invasive level of this technique is prohibitive to BP monitoring for the majority of applications and is typically left for diagnosis and monitoring of abnormal heart conditions.

Cuff-based methods are widely used in clinical applications, however they do not lend themselves to ubiquitous BP monitoring. This is due to the fact that the cuff-based methods measure BP during deflation, thus prohibiting continuous measurements. In addition, prolonged cuff inflation can lead to venous pooling and patient discomfort [4]. Common cuff-based methods are auscultation, oscillometry and volume clamping. Auscultation is a manual method which requires the clinician to listen to the Korotkoff sounds during cuff inflation. Special training is required for using this method and as a result is not favorable for at-home monitoring.

In oscillometry, the most commonly used clinical technique, a cuff is placed on the patient, usually on the arm or leg, and inflated to a pressure higher than systolic. Cuff pressure is deflated at a constant rate and oscillations in the cuff pressure are

mapped to diastolic to systolic pressures. Since measurements can only be taken during cuff deflation, continuous monitoring is not possible.

Volume clamping methods measure pulsatile unloading at zero transmural pressure. To accomplish this, a cuff is dynamically inflated to ensure zero transmural pressure thus enabling direct translation of arterial pressure to cuff pressure. Physically this method requires both a cuff and a photoplethysmography (PPG) sensor to operate. The PPG sensor optically obtains a blood volume measurement through measuring changes in light-absorption of the skin. The requirement of two devices for this method is undesirable for ubiquitous BP monitoring and as such volume clamping techniques are primarily used in research applications.

A non-cuff-based method, tonometry, is yet another method for measuring blood pressure. This technique requires a skilled clinician to manually compress an artery with a probe. The probe must be perpendicular to the compressed artery and the artery must be completely flattened so that pressure differences are clear. This method tends to be uncomfortable for the patient and remains mainly a research technique.

In sum, each technique currently has a shortcoming either by requiring a cuff, a skilled clinician to perform manually, or is invasive. Current work towards BP monitoring methods which address these issues is discussed in the next section.

1.3 Pulse Transit Time and Blood Pressure

Due to the aforementioned difficulties in directly measuring BP, research towards ubiquitous blood pressure monitoring is currently being pursued through measurement of a BP surrogate. The characteristics of a reliable and patient-accessible surrogate of blood pressure would include real-time changes to blood pressure and be easily measured by a single sensor (i.e., an app on a smartphone). Currently, interest is focused on pulse transit time (PTT), which is the measurement of time-delay between two arterial waveforms (usually a proximal wave and a distal wave).

PTT is known to be inversely related to BP through arterial stiffness [5] and has typically been measured by using the electrocardiogram (ECG) R-wave as a proximal (i.e., close to the heart) timing reference [6], [7], [8], [9], [10]. A distal (i.e., father away from the heart) reference may either be diastolic blood pressure (DBP) measured from one of the techniques mentioned above, or from the foot of a PPG waveform. However, some studies have shown the ECG R-wave to be an inaccurate marker of PTT [11], [12]. These studies have demonstrated the innacuracy of the ECG-R wave since it occurs at the start of heart isovolumentric contraction rather than left ventricular ejection. Thus this "PTT" includes the difference between these heart events known as pre-ejection period (PEP) in addition to the true PTT. While PTT is inversely correlated to blood pressure, PEP is not a true surrogate of blood pressure and is affected by other physical characteristics (e.g., myocardial contractility [13], [14]). Thus these previous methods of PTT estimation have been classified as the measurement of pulse arrival time (PAT) which is defined as

the sum of PEP and PTT. As a result, PAT is said to be inherently flawed as a blood pressure surrogate due to the inclusion of PEP. Recently, alternative proximal timing references for PTT measurement have been proposed, including use of the Ballistocardiogram (BCG) [5], [15], [16]. The next section shall review the potential for using the BCG as a proximal timing reference.

1.4 Ballistocardiogram: Use as a Proximal Timing Reference

1.4.1 Origins

The BCG, discovered in the 1800s by J.W. Gordon, is the measurement of the body's force response to the heart pumping blood [17]. At the time of discovery, there was much interest in the applications of the BCG as a cardiovascular health marker (see for example: [18], [19], [20], [21]). Measurement of the BCG was accomplished by suspending a patient on a platform and measuring the movement of the platform [22]. Various suspension platforms were developed in the mid-1950s: either on a direct bed, where the displacement of the patient is directly measured [23], [24], or on high [20], [25], or low frequency beds [26], [27], [28], where the frequency refers to the natural frequency of the measuring bed [29], [30], [31]. In each of these measurement devices, either the acceleration, velocity, or displacement of the bed may be measured. However the measurement of the BCG was cumbersome and lack of understanding of this waveform lead to loss of interest when medical imaging technologies emerged. It was not until recently, due to advancement in sensor technology, that interest in understanding the BCG mechanism and its applications

resumed. For clarity, the BCG waveform discussed henceforth shall be a force BCG comparable to the low-frequency acceleration BCG or high-frequency displacement BCG from previous works (See examples from [23], [24], [26], [27], [28]).

1.4.2 Relation to Cardiac Functions

Figure 1.1 illustrates the features of a BCG wave in a normal human. A discussion of the cardiovascular origins of each wave is provided since it is a goal of this thesis to validate these origins according to a model (discussed in a later chapter) presented in [1]. In conjunction, this thesis also aims to justify the basis of the BCG as a proximal timing reference for PTT and provide additional evidence for its superiority over ECG-based PAT techniques. Thus an understanding of BCG cardiac origins directs the development of a BCG-based PTT model.

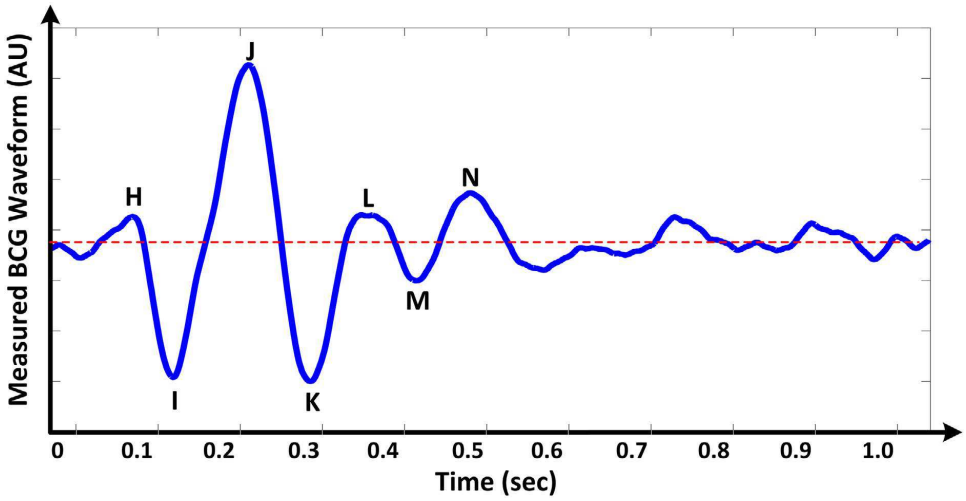

Figure 1.1: A typical BCG waveform adapted from [1]

According to [32], the H wave occurs at, or prior to, left ventricular ejection.

Thus the H wave is not a reasonable PTT proximal timing reference since it may also include a portion of PEP. Conversely, the I wave is attributed to the change in direction of blood movement from the headward direction to the footward direction [18], [32]. Thus the I wave is believed to occur due to blood movement near the top of the aortic arch, and is used as a proximal timing reference due to the adjacency of the aortic arch to the aortic value (approximately 6 cm [33]).

The origins of the J wave have been more difficult to attribute to cardiac features. However, it is generally agreed that the J wave is due to the deceleration of blood in the ascending aorta and aortic arch and acceleration of blood in the descending arteries [18], [32], [34].

The K wave origins have historically been even more puzzling than the J wave. Some have thought the K wave could simply be the recoil of the measuring bed from the J wave. Others have attributed the K wave to the slowing of blood in the main descending arterial segments and acceleration of blood flow in the legs [35]. This explanation is more likely since it was noted in [34] that many patients can have K waves larger in amplitude than the J wave.

The L, M, and N waves are less interesting in terms of this thesis since they are not related to early cardiac functions (i.e., they occur post-systole). Thus having no immediate relevance to the proximal reference timing for PTT.

1.5 Problem Definition and Goals

Addressing the lack of ubiquitous blood pressure monitoring techniques for early hypertension detection and long term monitoring would provide a significant improvement in patient health care. The development of a reliable and continuous blood pressure monitoring method which does not require the use of a cuff would provide a large contribution towards patient health care.

Pulse transit time has already been identified as a surrogate of blood pressure and can be non-invasively and continuously measured through the ECG and a PPG sensor. However the previously mentioned issues with this ECG-based method prevent the development of this method into a reliable monitoring system. This thesis seeks to explore an alternative, non-invasive method for PTT measurement. Since the BCG is directly related to the occurrence of the heart pumping blood, it lends itself as a proximal timing reference for PTT. The BCG-I wave occurs near the aortic value and would ideally provide a better proximal timing reference for PTT than conventional ECG-based methods. Thus this thesis seeks to explore this timing reference and compare it to conventional methods.

However the BCG-I wave does not occur exactly at left ventricular ejection. Thus a PTT measured with this reference is expected to be an improvement to current methods but true PTT remains un-captured. Left ventricular ejection is known to occur between the H wave and I wave. Thus if it was possible to identify the occurrence of blood ejection in terms of the BCG, further improvement in the use of BCG-based PTT would be seen.

Thus this thesis aims to address the lack of ubiquitous blood pressure monitoring through PTT in the following manner:

- Directly compare BCG-based PTT, measured as the time-delay between the BCG-I wave and distal PPG wave, to conventional ECG-based PAT by evaluating the correlation to BP of each time-delay. This is denoted as a Signal-Based Approach.
- Evaluate the accuracy of BCG-based PTT by the Signal-Based Approach as a blood pressure predictor.
- Develop a model for BCG-based PTT which would identify occurrence of left ventricular ejection in the BCG wave. This is denoted as the Model-Based Approach.
- Compare Model-based PTT to Signal-based PTT and Conventional PAT and assess the accuracy of each predictor.

The main assumption of this thesis is in regard to the Model-Based Approach. Namely, it is assumed that the main mechanism of the BCG generation is forces by blood pressure. Any contribution by other forces by blood flow are assumed to be negligible. This assumption was deemed reasonable since generation of BCG-like waveforms was accomplished in [1] which found flow contribution to the waveform to be negligible.

Chapter 2: Data Sets

2.1 Collection

Data collected from human subjects were studied from an IRB-approved Georgia Institute of Technology and Michigan State University study (reported in [36]). Six physiologic waveforms were collected from 22 young, healthy subjects (age range: 25 $\pm$ 3.5 years; gender: 19 males; height: 177 $\pm$ 11 cm; weight: 75 $\pm$ 15 kg). The following were measure:Two PPG waveforms, one collected at the instep of the foot ("Foot PPG") and one collected from the left index finger ("Finger PPG"), a three-lead ECG, a Finapres BP (measured at the left middle finger), a BCG (collected from a weighing scale-like system first developed in [37]), and an eight-lead impedance cardiography (ICG). Data were collected at a sampling rate of 2kHz.

Methods of data collection occurred were as follows: First a baseline recording was taken while the subject was at rest ("R1") for 60sec, next the subject was required to complete mental arithmetic ("MA") calculations for 60sec consisting of consecutive arithmetic to raise their blood pressure (i.e., given the number 123, the subject was asked to add the digits and increase the number by that sum: 123 + 6 = 129. The new number was used as the input to the next iteration). This intervention was followed by a second resting period of 60sec to allow the subjects

BP to return to baseline ("R2"). A second intervention of a cold presser ("CP") was executed by submerging the subjects right hand into 4 °C water for 60sec. The third resting period lasted for 120sec to allow a return to baseline ("R3"). The subject proceeded to get off of the scale and perform a stair-climbing exercise for 60sec, after which they returned to the scale and recording of the post-exercise ("PE") waveforms resumed.

Each intervention was chosen to induce an increase in BP, representative of normal daily activities, but modify PEP in different ways [38], [39], [40], [41], [42]. That is, the MA intervention would increase BP while decreasing PTT and PEP. However the CP intervention would increase BP while decreasing PTT and increasing PEP. Finally the PE intervention would increase BP and decrease both PEP and PTT. Since PAT is the sum of PEP and PTT, it was expected that ECG-based PAT would become an unreliable predictor of BP across all interventions while PTT would remain a reliable marker.

2.2 Processing

Processing of this data was accomplished by band-pass filtering the BCG waveform with first-order Butterworth filters of 0.5Hz and 10Hz cutoff frequencies. The BCG waveform was smoothed by an exponential moving average. Outlier beats were identified and removed. The method by which this was accomplished was to compare time-delays of each beat with the mean and standard deviation of previous beat time-delays. A beat was removed if any time delay occurred outside of the

deviation band of the previous beats.

After outlier removal, representative beats were selected for each intervention which accomplished the greatest BP change. That is, a total of five beats from each intervention were selected which corresponded to the lowest average DBP in the resting interventions and the highest average DBP in the MA, CP and PE interventions. For the model-based approach, the waveforms from selected beats were then high-pass filtered at 1kHz prior to use in the model. This was necessary to ensure a zero-mean for the model, whereas such a requirement was not necessary for the signal-based approach.

These representative beats were used for measurement of PTT, PAT, and PEP. The following chapter shall discuss a signal-based approach (i.e., simple feature extraction) for measurement of PTT. This BCG-based PTT shall be compared to PAT as a marker of BP. After PAT is shown to be unreliable due to PEP, and that PTT is a superior marker by the signal-based method, a model-based approach shall be developed. The goal of this model-based approach is to determine if a truer PTT can be extracted using known relationships between the BCG and cardiac events. To conclude, each approach shall be compared and suggestions for future work in this topic shall be made.

2.2.1 Limitations

A limitation of the collected data is that the BCG signal was collected from the patients in the upright, standing posture. This measurement is highly susceptible

to motion artifacts and filtering techniques where used to limit the impact of these artifacts. However, it would have been ideal to collect the BCG while the subjects were in the supine (i.e., laying down) position. This would have limited the impact of motion artifacts, and in addition ensured no blood pressure changes within the body due to elevation of the subject. That is, all blood pressure changes would be due to physiological changes and not elevation gradients.

Chapter 3: Signal-Based Approach

3.1 Methods

The extraction of PTT, PAT, and PEP time-delays are summarized in Figure 3.1. Feature detection of each wave feature occured as follows: BCG I wave identification was accomplished by first detecting the prominent J wave and then identifing the first peak previous to that as the I wave. The popular Pan-Tompkins method was used for ECG-R wave detection and an intersecting tangent method was used to detect the foot of PPG waveforms.

PAT was measured as the time-delay between ECG R-peak and the Finger PPG ("Conventional PAT"). Since it is the goal of this study to compare conventional PAT with a BCG-based PTT, two PTT measurements were made. First, the time-delay between the BCG-I wave and the Finger PPG ("Arm PTT") for a direct comparison to PAT. Second, since the BCG is related to descending artery events, the time-delay between the BCG-I wave and the Foot PPG ("Scale PTT") was also measured. It was hypothesized that, since the BCG-I wave is attributed to forces occurring at the aortic arch, the Scale PTT would be a more reliable marker of BP than Arm PTT. PEP was defined as the time-delay between the ECG-R wave and the peak of the BCG I wave. Diastolic ("DBP") and systolic ("SBP")

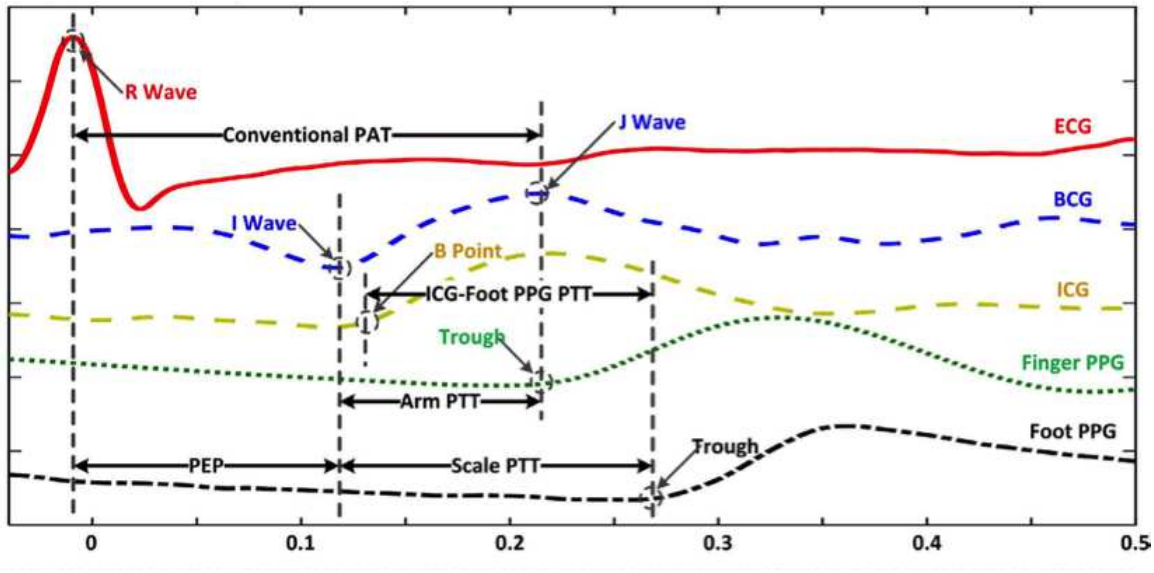

Figure 3.1: Signal-Based Feature Extraction. Taken from [36]. An example beat showing feature extraction techniques.

blood pressures were also extracted from the Finapres BP for each beat. Toe PAT was not considered for this comparison since ECG-based PAT has historically been measured from a finger PPG distal reference [5], [43].

Time-delays from the five identified beats were averaged to provide a robust estimate for that intervention. The magnitude of these time-delays ranged from approximately 50ms to 120ms. This resulted in 6 data points (one for each intervention) for each PTT (Arm and Scale), PAT, PEP and BP for each subject. Prediction of DBP and SBP then proceeded by computing a linear regression between the measured time-delays and BP for the subject and then predicting BP from the regression.

3.2 Results and Discussion

3.2.1 Correlation Results

Table 3.1 shows the correlation results of each subject for conventional PAT, arm PTT, scale PTT and PEP. Correlations were computed using the Pearson correlation coefficient between measured time-delays and BP.

Table 3.1: Signal-Based Approach Results

	Conv. PAT		Arm PTT		Scale PTT		PEP	
Subject	DBP	SBP	DBP	SBP	DBP	SBP	DBP	SBP
1	-0.56	-0.62	-0.73	-0.77	-0.92	-0.92	-0.61	-0.67
2	-0.58	-0.80	-0.84	-0.85	-0.88	-0.93	-0.52	-0.81
3	-0.10	-0.27	-0.88	-0.82	-0.92	-0.80	0.30	0.13
4	-0.70	-0.60	-0.91	-0.86	-0.89	-0.85	-0.48	-0.38
5	-0.64	-0.74	-0.78	-0.84	-0.79	-0.74	-0.35	-0.46
6	-0.53	-0.49	-0.89	-0.82	-0.80	-0.85	0.04	-0.08
7	-0.53	-0.65	-0.95	-0.94	-0.84	-0.80	-0.05	-0.14
8	-0.72	-0.74	-0.65	-0.67	-0.74	-0.75	-0.44	-0.52
9	-0.71	-0.75	-0.90	-0.85	-0.78	-0.84	0.19	-0.13
10	-0.93	-0.89	-0.69	-0.61	-0.79	-0.62	-0.80	-0.81
11	-0.69	-0.90	-0.78	-0.84	-0.77	-0.94	-0.47	-0.70

Continued on next page

Table 3.1 – *Continued from previous page*

	Conv. PAT		Arm PTT		Scale PTT		PEP	
Subject	DBP	SBP	DBP	SBP	DBP	SBP	DBP	SBP
12	-0.52	-0.75	-0.36	-0.18	-0.76	-0.89	-0.43	-0.71
13	-0.74	-0.87	-0.67	-0.66	-0.62	-0.50	-0.78	-0.79
14	-0.75	-0.62	-0.49	-0.51	-0.84	-0.80	-0.67	-0.43
15	-0.71	-0.75	-0.66	-0.61	-0.91	-0.92	-0.52	-0.55
16	-0.54	-0.58	-0.87	-0.86	-0.60	-0.63	-0.34	-0.31
17	-0.39	-0.49	-0.77	-0.77	-0.92	-0.94	-0.03	-0.05
18	-0.20	-0.38	-0.34	-0.36	-0.63	-0.24	0.11	-0.32
19	-0.51	-0.70	-0.60	-0.77	-0.81	-0.92	-0.50	-0.69
20	-0.59	-0.62	-0.57	-0.56	-0.80	-0.84	-0.20	-0.29
21	-0.60	-0.49	-0.86	-0.87	-0.79	-0.92	-0.14	0.09
22	-0.96	-0.92	-0.96	-0.44	-0.87	-0.93	-0.77	-0.93
Mean	**-0.60**	**-0.66**	**-0.71**	**-0.70**	**-0.80**	**-0.80**	**-0.34**	**-0.43**
SE	**0.04**	**0.04**	**0.04**	**0.04**	**0.02**	**0.04**	**0.07**	**0.07**

It is clear that overall, both arm PTT and scale PTT outperform conventional PAT. These results show that PAT had varying performance in BP correlation from subject to subject. In one-third of the subjects, PAT performed poorly due to poor PEP correlation to BP. Another one-third of the subjects saw poor PAT performance due to the arm PTT component. This is believed to occur due to smooth

muscle contractions in the arm [44]. In the remaining one-third of the subjects PAT performed well. Thus PAT is susceptible to both of its components and depends heavily on their synchronous performance.

3.2.2 Verification of Time-Delay Response

A key component of performing this study was ensuring the variable change in PEP with respect to BP across interventions. Figure 3.2 shows the average results of all 22 subjects for each intervention versus DBP (results are similar for SBP). The inverse relationship between PEP and DBP is maintained in the first 3 interventions. However, as expected PEP changes proportionally to DBP in the CP intervention thus causing a break-down of the relationship. In addition PEP exhibits a significant over-response to the PE intervention in relation to DBP, thus causing the correlation to degrade further.

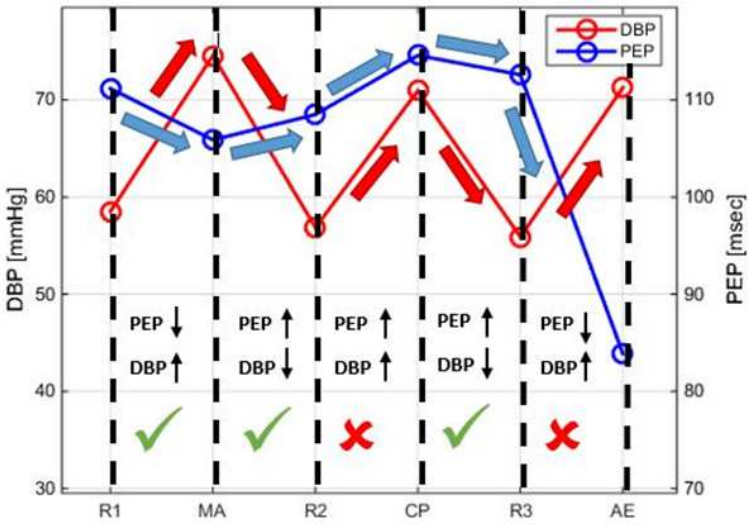

Figure 3.2: Average PEP versus DBP.

Figures 3.3(a) and 3.3(b) show the average response of scale PTT and conventional PAT to DBP across the interventions. The influence of PEP on conventional PAT is very clear in the CP and PE regions where PAT under-responds and over-responds, respectively. In contrast, average scale PTT follows the changes in DBP in both magnitude and direction.

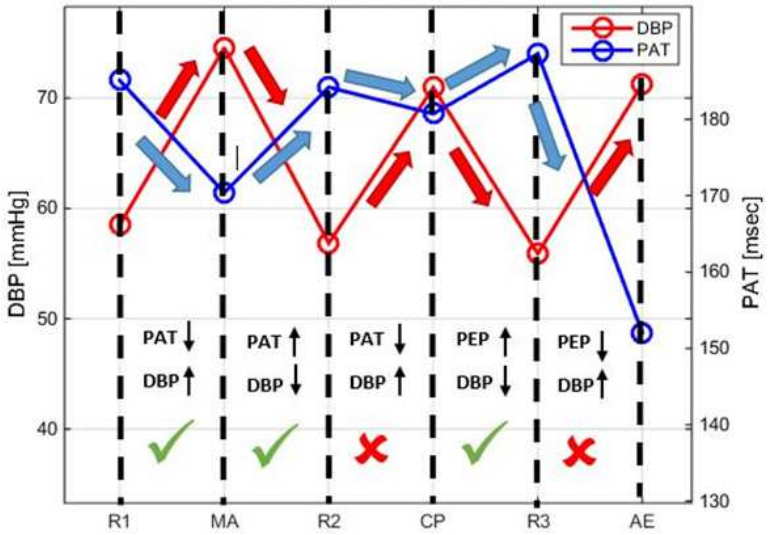

(a) Average Conventional PAT vs. DBP

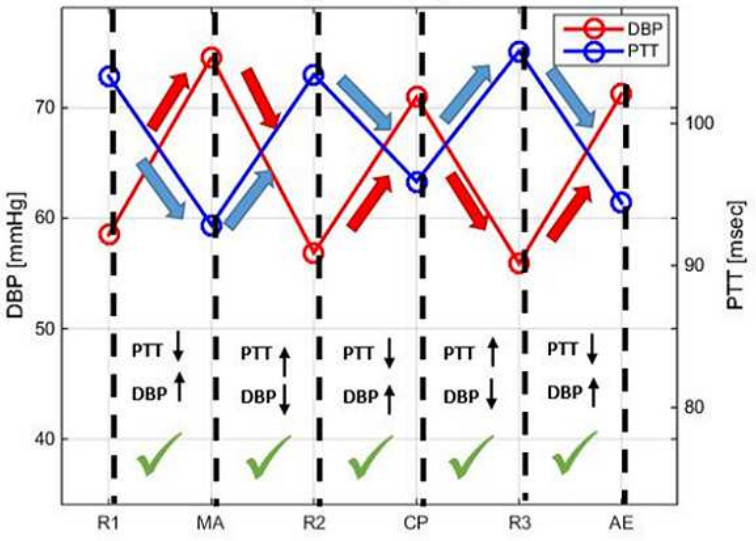

(b) Average Scale PTT vs. DBP

Figure 3.3: Average Intervention Response vs. DBP

3.2.3 BP Prediction Errors

With each of the subjects, calibration of predicted BP with measured BP was performed to yield a best-case prediction of BP in each time-delay. Figure 3.4 summarizes these results for scale PTT and conventional PAT in terms of base-case predicted BP versus measured BP and a Bland-Altman plot of the prediction errors. For each conventional PAT and scale PTT, one outlier subject was removed prior to error determination for this best-case scenario.

Even with removal of one outlier subject for each scale PTT and conventional PAT, scale PTT continued to be a superior marker. In terms of RMSE for DBP and SBP, scale PTT was much smaller (7.6mmHg and 11.8 mmHg, respectively) than RMSE for conventional PAT (14.6mmHg and 18.5mmHg, respectively). Indeed it is easy to see the overall lower error in scale PTT according to the Bland-Altman plots. The spread of errors in scale PTT for DBP is much smaller than conventional PAT; while the difference of spread is less drastic in SBP, but overall scale PTT still surpasses conventional PAT.

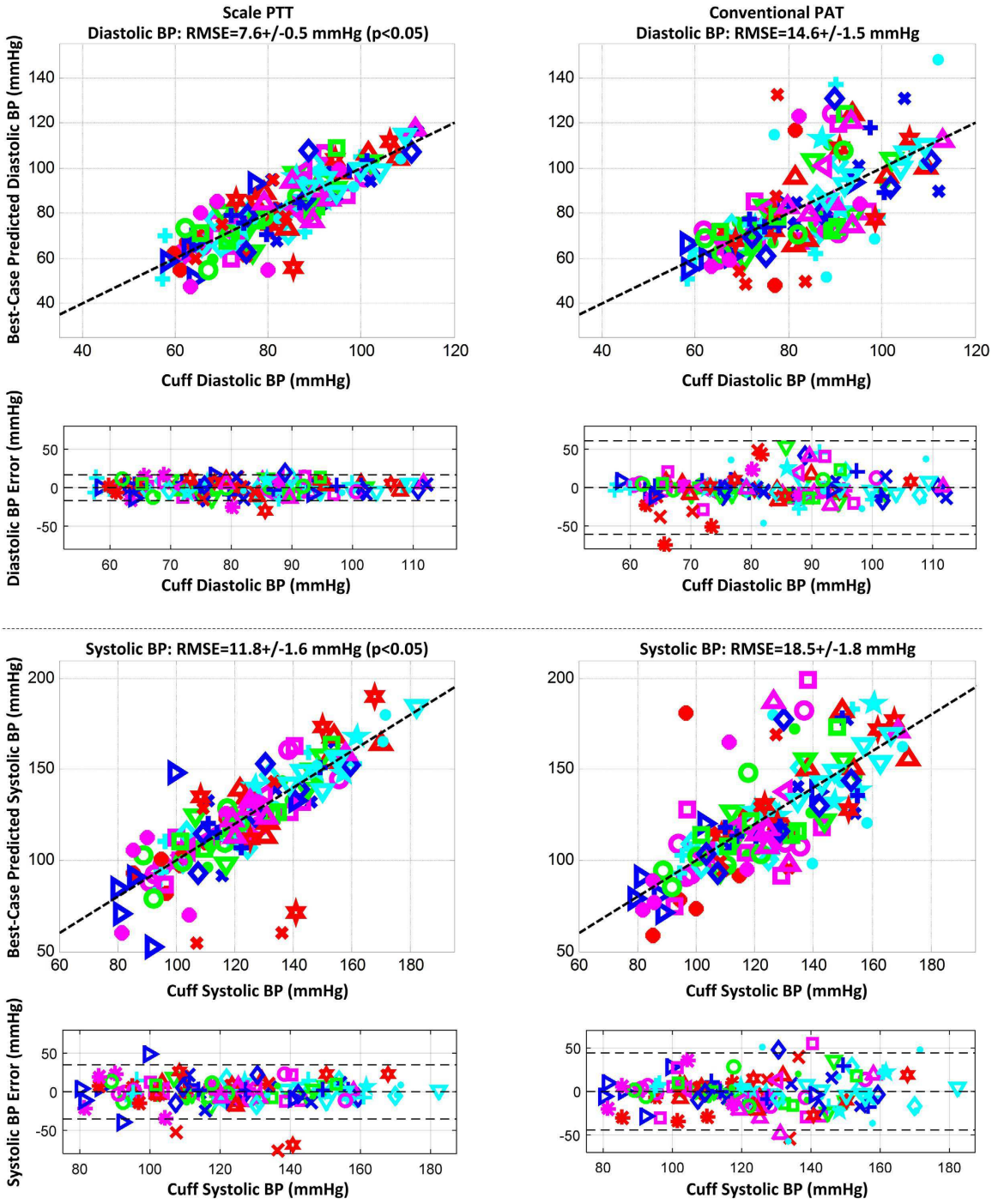

Figure 3.4: Best-case BP prediction

3.3 Conclusions

It can clearly be concluded from this signal-based method, that BCG-I PTT is a more robust and accurate predictor of BP than conventional ECG-based PAT. The reason for this superiority stems from the inclusion of PEP in conventional PAT, which is not a reliable BP marker. In addition, arm PTT can further lower the accuracy of PAT as a predictor.

The next chapter shall build on this demonstration of BCG-based PTT for BP prediction by developing a model for PTT. This model aims to further elucidate the physiological origins of the BCG wave and, therefore, strengthen the the use of BCG-based PTT for ubiquitous BP monitoring.

Chapter 4: Model-Based Approach

4.1 BCG Mechanism Model

4.1.1 Ballistocardiogram Relationship to Arterial Pressures

A model was provided in [1] which elucidated the origins of the BCG wave. This model, which is the foundation for the model-based approach of this thesis, related three pressures along the descending arteries to BCG wave features. In [1], two of the pressures were measured directly from human catheterization near the aortic arch and femoral arteries. The third pressure was generated by imposing a time-delay on the measured aortic arch pressure to estimate the ascending aortic pressure. These three pressures were divided into two tubes, one for ascending blood flow and one for descending flow. Figure 4.1 illustrates the pressure locations.

Since the BCG is the measurement of the body's reaction to blood forces, the pressures were converted to arterial forces by multiplication of mean areas for each tube. These areas were determined by averaging the inlet and outlet areas for each tube derived from population mean values. The estimated BCG wave was generated by subtracting the net force in the ascending tube from the net force in the descending tube, yielding the overall force in the descending direction. Example

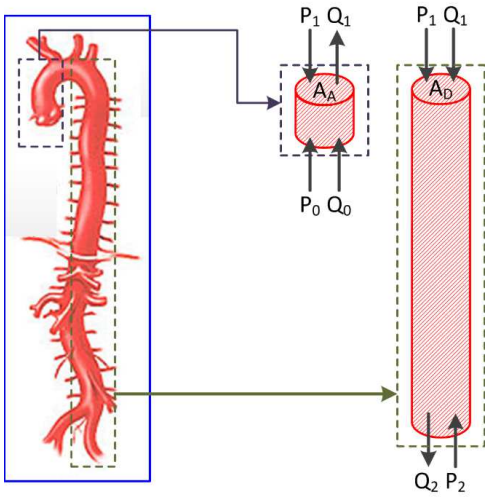

Figure 4.1: Location of blood pressure forces from [1]. The ascending aorta is represented by the shorter tube with a single cross-sectional area A_A. The descending aorta is represented by the longer tube with single cross-sectional area A_D

results of this model are shown in Figure 4.2.

It can be seen that the I wave occurs near the maximum difference in ascending aortic pressures. This follows the previous discussion where the I wave was assumed to occur near the aortic arch. In this model, the two most proximal pressures have their diastolic occur before the I wave peak. This is important to note since the BCG-I wave was used as the proximal timing reference for PTT, however the most proximal waveform has its diastolic prior to the the I wave. This suggests that there is room for improvement from the signal-based approach in terms of estimating true aortic PTT from the BCG.

The J wave occurs near the systolic of the second pressure, P_1, and during the upstroke of the most distal pressure, P_2. This agrees with the previous belief that the J wave occurs due to the deceleration of blood in the ascending aorta and

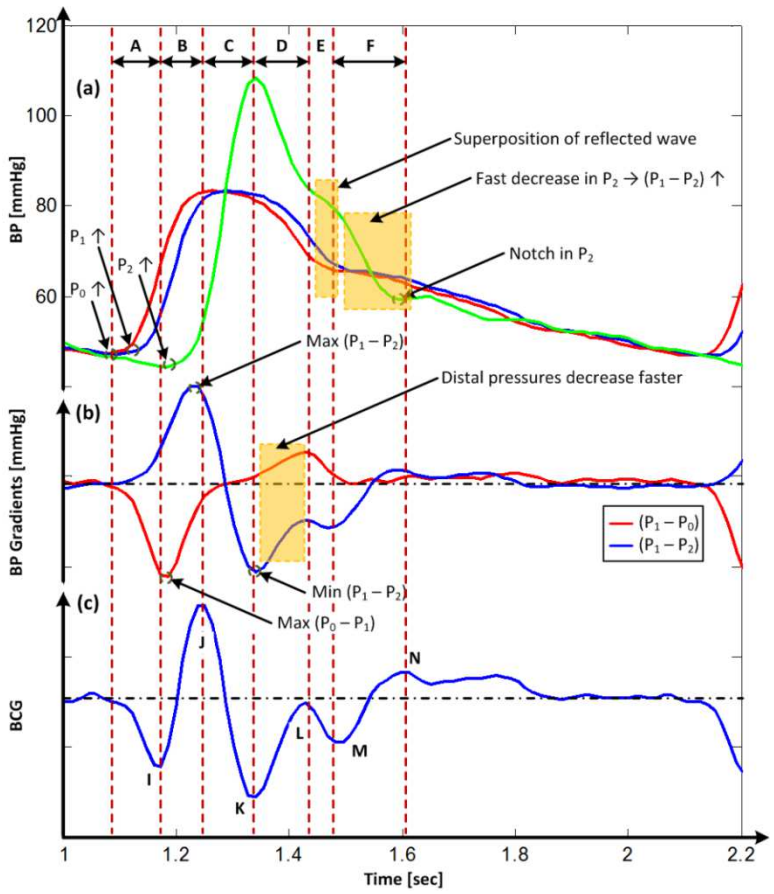

Figure 4.2: Generation of BCG-like waves from arterial pressures

acceleration of blood in the descending arteries. Finally, the K wave occurs near the systolic of the most distal pressure, agreeing with the assertion that the K wave occurs due to acceleration of blood in the lower arteries.

These BCG wave timings, in relation to occurrence of cardiac pressure features, shall provide timing guidelines for the model proposed in this thesis. Details on how these guidelines are used are provided in a later section. The next section shall briefly deviate from BCG modeling to describe a technique for arterial pressure estimation. Afterwards, this BCG mechanism model shall be combined with arterial pressure

estimation techniques to present a BCG-based model for PTT estimation.

4.1.2 Transmission Line Theory for Arterial Hemodynamics

Transmission line theory has commonly been applied to arterial hemodynamics to relate proximal and distal pressure and flow waveforms [45], [46], [47], [48], [49], [50], [51], [52]. The theory states that pressure waves are 1) the sum of forward and backward traveling pressure waves and 2) proximal and distal waves are related to each other through a time offset and reflection coefficient. The forward traveling distal wave (P_{f1}) is the time delay of the forward traveling proximal wave (P_{f0}), where the time delay is the pulse transit time (PTT) of the wave. The backward traveling distal wave (P_{b1}) is simply the reflection of the forward traveling distal wave which is given by the reflection coefficient. This reflection coefficient is determined by an approximation of the load to the tube from the remaining distal arteries. Finally, the backward traveling proximal wave (P_{b0}) is the time delay of the backward traveling distal wave. From these approximations, the following transfer function between the proximal and distal wave, in the Laplace domain, is found (See Appendix A for a full derivation):

$$\frac{P_p(s)}{P_d(s)} = \frac{e^{\tau s} + e^{-\tau s}\Gamma(s)}{1 + \Gamma(s)} \tag{4.1}$$

Where τ is the PTT between the proximal and distal pressures and Γ is the tube-load reflection coefficient. For the purposes of this thesis, the tube-load model shall be the well-known 3-element Windkessel model [50], [53], [54], [55]. This model

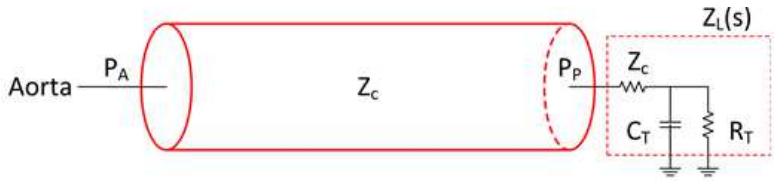

Figure 4.3: Diagram of single tube Windkessel Tube-Load model adapted from [57]

expresses the distal load of the modeled artery in terms of the impedance, resistance and capacitance of the distal arteries (See Figure 4.3) [56], [57]. These parameters are expressed by the reflection coefficient Γ in the following equation:

$$\Gamma(s) = \frac{Z_L(s) - Z_C}{Z_L(s) + Z_C} \tag{4.2}$$

Where Z_C is the extimated tube characteristic impedance and the total Windkessel impedance, Z_L, is given by:

$$Z_L(s) = Z_C + \frac{R_T}{R_T C_T s + 1} \tag{4.3}$$

Parameterization of the Windkessel tube-load model may be accomplished through either "lossy" or "lossless" models (i.e., blood volume either decreases or remains constant throughout transmission, respectively). In [47] it was shown that "lossy" models provide improved accuracy, however these improvements were small and increased only slightly as the blood pressure loss increased. The "lossy" model also requires additional model parameters to be estimated, thus increasing the computational cost of the model parameter optimization. Since the "lossless" tube load

model has been shown to have reliable results for the prediction of central blood pressure compared to a "lossy" model, this thesis shall use the "lossless" model.

The "lossless" parameterization of the tube-load model is accomplished by two lumped parameters η_1 and η_2. Substituting Equation 4.3 into Equation 4.2, the parameterization is:

$$\Gamma = \frac{R_T}{2Z_C R_T C_T s + (2Z_C + R_T)} = \frac{\eta_2}{s + \eta_1} \tag{4.4}$$

where

$$\eta_1 = \frac{2Z_C + R_T}{2Z_C R_T C_T} \tag{4.5}$$

and

$$\eta_2 = \frac{R_T}{2Z_C R_T C_T} \tag{4.6}$$

Substituting this parameterization into Equation 4.1, a proximal pressure may be expressed in terms of a distal pressure by:

$$P_p(s) = \frac{e^{\tau s}(s + \eta_1) + e^{-\tau s}\eta_2}{s + \eta_1 + \eta_2} P_d(s) \tag{4.7}$$

The next section shall expand upon the BCG mechanism model by incorporating transmission line theory to estimate the BCG from a single measured pressure wave.

4.1.3 BCG-Based PTT Model

The model from [1] generated the BCG wave by subtracting the net force in the ascending tube from the net force in the descending tube, yielding the overall force in the descending direction as shown in Equation 4.8.

$$BCG = -A_A(P_0 - P_1) + A_D(P_1 - P_2) \tag{4.8}$$

Where A_A represents the mean arterial area for the ascending tube and A_D represents the mean arterial area for the descending tube. Note the contribution to arterial forces from blood flow was found to be dominated by the pressure forces which resulted in flow-based forces being neglected in this model.

Incorporating the relationship between proximal and distal pressures developed earlier, P_0 and P_1 can be estimated from P_2 as follows:

$$P_1(s) = \frac{e^{\tau_2 s}(s + \eta_1) + e^{-\tau_2 s}\eta_2}{s + \eta_1 + \eta_2} P_2(s) \tag{4.9}$$

Where τ_2 is the strictly positive time-delay from P_1 to P_2. Repeating for the estimation of P_0 from P_2:

$$P_0(s) = \frac{e^{(\tau_1+\tau_2)s}(s + \eta_1) + e^{-(\tau_1+\tau_2)s}\eta_2}{s + \eta_1 + \eta_2} P_2(s) \tag{4.10}$$

Where τ_1 is defined as the strictly positive time-delay from P_0 to P_1 and the sum of τ_1 and τ_2 is the time-delay from P_0 to P_2.

Substituting these equations into 4.8 yields the following transfer function:

$$\begin{aligned} BCG(s) &= \Bigg(- A_A \frac{e^{(\tau_1+\tau_2)s}(s+\eta_1) + e^{-(\tau_1+\tau_2)s}\eta_2}{s+\eta_1+\eta_2} \\ &+ (A_A + A_D)\frac{e^{\tau_2 s}(s+\eta_1) + e^{-\tau_2 s}\eta_2}{s+\eta_1+\eta_2} - A_D \Bigg) P_2(s) \end{aligned} \tag{4.11}$$

At this point, it is important to note the exact physical location of each pressure in the BCG model is unknown, most specifically the model-expected location of P_2. However, from the guidelines for pressure timings, the model requires P_2 systole to occur at or near the K wave and P_2 diastole prior or at the I wave. In order for this model to appropriately estimate the BCG, it is necessary to ensure the input pressure has these characteristics. It very difficult to guarantee this exact timing when collecting pressure data. To compensate for this measurement offset, the addition of a third pressure, denoted henceforth by P_3, to the BCG model is required. P_3 shall be the measured pressure waveform which may occur either proximal, distal or exactly at the BCG model-expected P_2.

It is expected that any time delay between P_3 and P_2 would be small (i.e., less than 30ms). A time-delay of 30ms represents a pulse displacement of approximately 15-20cm in distal arteries. Thus implementation of transmission line theory between P_3 and P_2 would be unnecessary and generate additional parameters for the model to estimate. Thus, any time delay between P_3 and P_2 shall be implemented through a simple shift in pressure timing, maintaining all other features of the wave. This is

explicitly expressed in the following equation.

$$P_2 = e^{\tau_3 s} P_3 \tag{4.12}$$

Where τ_3 may be either positive or negative. A positive τ_3 value shall indicate a proximal shift of P_3 and a negative τ_3 value shall indicate a distal shift. Figure 4.4 illustrates the location of each of the pressures.

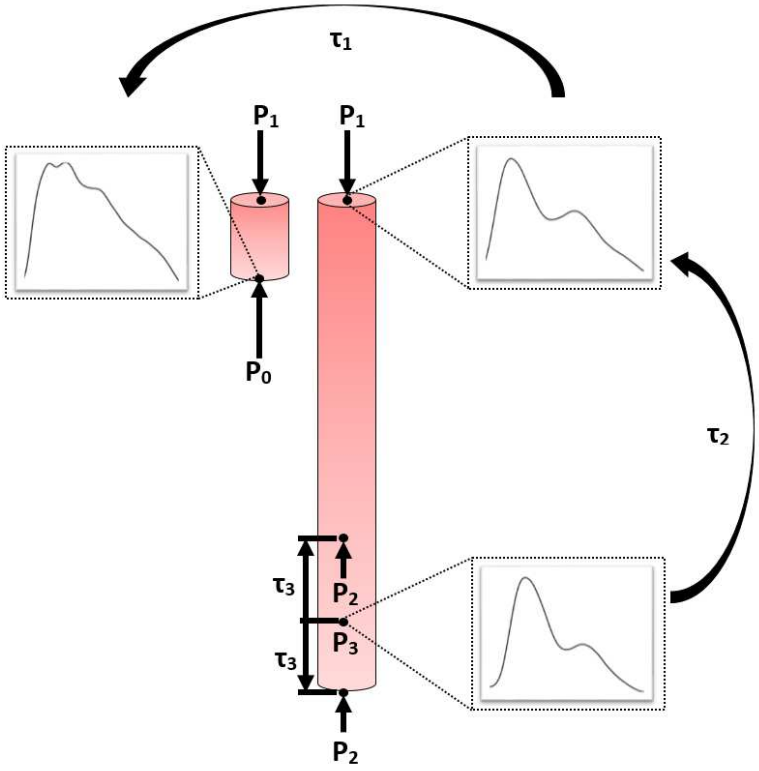

Figure 4.4: Pressure Locations of Model-Based Approach. τ_3 may be a positive (i.e., proximal) or negative (i.e., distal) shift of P_3 to P_2. τ_2 is a strictly positive shift of P_2 to P_1 via transmission line theory, as is τ_1 a positive value for a transmission line shift from P_1 to P_0.

Incorporation of P_3 into the Equation 4.11 yields the following:

$$BCG(s) = \left(-A_A \frac{e^{(\tau_1+\tau_2+\tau_3)s}(s+\eta_1) + e^{(\tau_3-\tau_1-\tau_2)s}\eta_2}{s+\eta_1+\eta_2} + (A_A+A_D)\frac{e^{(\tau_2+\tau_3)s}(s+\eta_1) + e^{(\tau_3-\tau_2)s}\eta_2}{s+\eta_1+\eta_2} - A_D e^{\tau_3 s} \right) P_3(s) \quad (4.13)$$

The estimated PTT from this model may be a combination of τ_1,τ_2, or τ_3 estimated by the model. Determination of which combination to be used shall be elucidated in a later section.

4.1.3.1 Model Variants

This thesis shall propose two variants on the model developed above. The first model shall assume τ_3 is an unknown parameter and use system identification methods to estimate its value. This would maintain the transfer function from Equation 4.13 and have a total of 7 parameters which the system must identify $(\tau_1, \tau_2, \tau_3, \eta_1, \eta_2, A_A, A_D)$.

The second variant shall set τ_3 to a value determined from patient specific data. That is, since the mechanism model suggests that P_2 systole occurs very near the peak of the K wave, τ_3 shall be estimated to equal the beat-to-beat difference between the systole of the measured distal pressure and the measured K wave. This results in the transfer function of Equation 4.11 with a total of 6 parameters for system identification $(\tau_1, \tau_2, \eta_1, \eta_2, A_A, A_D)$.

The two variants shall henceforth be distinguished by denoting the first variant

by "Full Parameter Model" (FPM) in which τ_3 is a system identified parameter and second variant by the "Reduced Parameter Model"(RPM) where τ_3 is a physiologically obtained value. Both models shall be explored and compared in the remaining sections of this thesis.

4.1.3.2 Discretization of Model

Discretization of the FPM may be accomplished through the Z-transform and approximating $\tau_i s$ by equating to $n_i(z-1)$. Full details on this discretization are provided in Appendix A.

$$\begin{aligned} BCG[k+1] &= \Big(1-\frac{\eta_1+\eta_2}{F_s}\Big)BCG[k] - A_A P_3[k+n_1+n_2+n_3+1] \\ &+ A_A\Big(1-\frac{\eta_1}{F_s}\Big)P_3[k+n_1+n_2+n_3] - A_A(\Big(\frac{\eta_2}{F_s}\Big)P_3[k-n_1-n_2+n_3] \\ &+ (A_A+A_D)P_3[k+n_2+n_3+1] + (A_A+A_D)\Big(\frac{\eta_1}{Fs}-1\Big)P_3[k+n_2+n_3] \\ &+ (A_A+A_D)(\frac{\eta_2}{F_s})P_3[k-n_2+n_3] - A_D P_3[k+n_3+1] \\ &+ A_D\Big(1-\frac{\eta_1+\eta_2}{F_s}\Big)P_3[k+n_3] \end{aligned} \tag{4.14}$$

Similarly, the discretization of the RPM yields the following equation (See Appendix A):

$$
\begin{aligned}
BCG[k+1] &= \Big(1-\frac{\eta_1+\eta_2}{F_s}\Big)BCG[k] - A_A P_2[k+n_1+n_2+1] \\
&+ A_A\Big(1-\frac{\eta_1}{F_s}\Big)P_2[k+n_1+n_2] - A_A(\Big(\frac{\eta_2}{F_s}\Big)P_2[k-n_1-n_2] \\
&+ (A_A+A_D)P_2[k+n_2+1] + (A_A+A_D)\Big(\frac{\eta_1}{Fs}-1\Big)P_2[k+n_2] \\
&+ (A_A+A_D)(\frac{\eta_2}{F_s})P_2[k-n_2] - A_D P_2[k+1] \qquad (4.15) \\
&+ A_D\Big(1-\frac{\eta_1+\eta_2}{F_s}\Big)P_2[k]
\end{aligned}
$$

The following section shall explore each model to facilitate understanding of the system parameters and the sensitivity of the model to each parameter.

4.2 System Identification

4.2.1 Identifiability

Prior to application of these models to data, it is vital to ensure all parameters are uniquely identifiable. To facilitate this, a pseudo-linear regression is applied to the discrete form of the FPM as follows:

$$BCG[k] = \Phi\Theta \qquad (4.16)$$

Where

$$\Phi = \begin{bmatrix} BCG[k-1] \\ -P_3[k+n_1+n_2+n_3] \\ P_3[k+n_1+n_2+n_3-1] \\ -P_3[k-n_1-n_2+n_3-1] \\ P_3[k+n_2+n_3] \\ P_3[k+n_2+n_3-1] \\ P_3[k-n_2+n_3-1] \\ -P_3[k+n_3] \\ P_3[k+n_3-1] \end{bmatrix}^T \tag{4.17}$$

$$\Theta = \begin{bmatrix} 1-\frac{\eta_1+\eta_2}{F_s} \\ A_A \\ A_A\left(1-\frac{\eta_1}{F_s}\right) \\ A_A\left(\frac{\eta_2}{F_s}\right) \\ (A_A+A_D) \\ (A_A+A_D)\left(\frac{\eta_1}{Fs}-1\right) \\ (A_A+A_D)(\frac{\eta_2}{F_s}) \\ A_D \\ A_D\left(1-\frac{\eta_1+\eta_2}{F_s}\right) \end{bmatrix} \tag{4.18}$$

From this form, it can be clearly seen that all parameters can be uniquely estimated from the coefficient vector Θ, and in fact the system is overdetermined. A_A can be found from the coefficients of $-P_3(k+n_1+n_2+n_3)$, A_D can be found from the coefficients of $P_3(k+n_3)$, η_1 can be found from the coefficients of $P_3(k+n_1+n_2+n_3-1)$ and $-P_3(k+n_1+n_2+n_3)$, and finally η_2 can be found from the coefficients of $-P_3(k+n_1+n_2+n_3)$ and $-P_3(k-n_1-n_2+n_3-1)$.

An eigenvalue decomposition is performed on the FPM model for each subject and intervention. Table 4.1 shows the mean and standard deviation of the eigenvalues and Figure 4.5 shows the mean associated eigenvectors. It can clearly be seen from Figure 4.5 that all of the regressors are explored by one or more of the eigenvectors (i.e., the last three regressors are excited by the first and second eigenvectors). In addition, with the exception of the first regressor, the eigenvalues are large in magnitude and thus we expect the second through ninth regressors to

be estimated accurately.

Table 4.1: Eigenvalue Decomposition of FPM

Eigenvalues in Mean (SD)								
λ_1	λ_2	λ_3	λ_4	λ_5	λ_6	λ_7	λ_8	λ_9
2.13 (2.15)	1.43E5 (3.69E5)	6.84E5 (9.65E5)	1.98E6 (1.97E6)	1.46E8 (2.33E8)	4.99E8 (6.92E8)	2.55E9 (1.44E9)	5.08E9 (2.65E9)	8.86E9 (4.68E9)

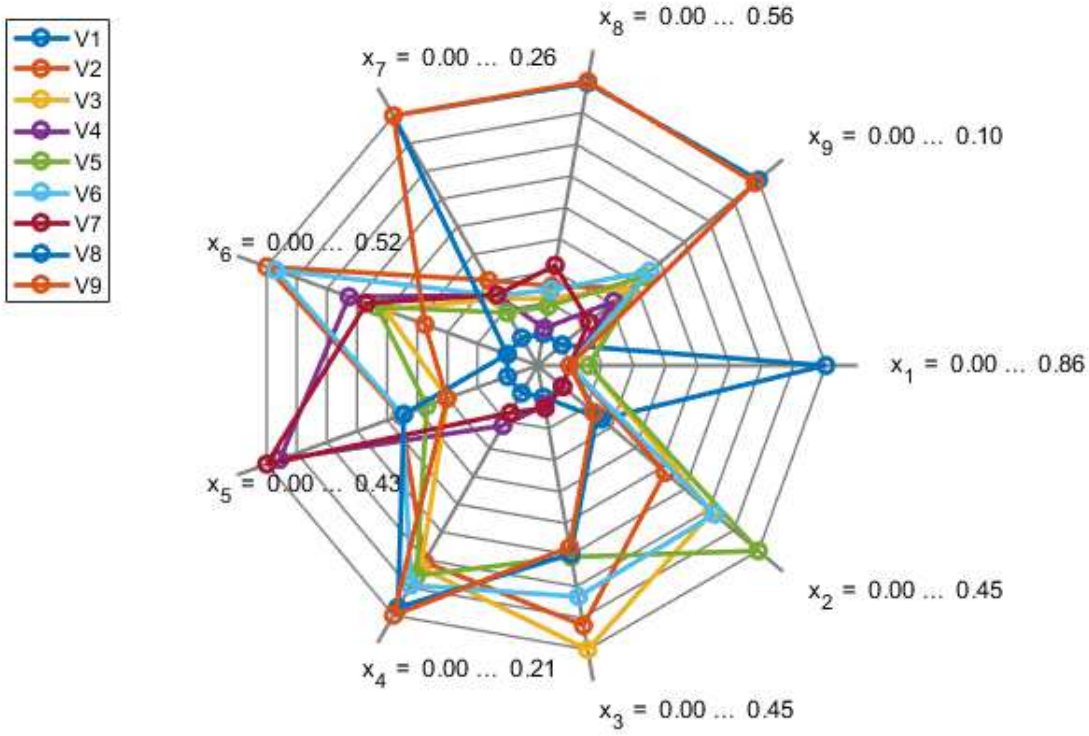

Figure 4.5: Eigenvectors for FPM Variant

The coefficients of the pseudo-linear regression of the RPM are the same as the LPM model and thus the identifiability is very similar. The regressor vector Φ is the only change and is provided below.

$$\Phi = \begin{bmatrix} BCG[k-1] \\ -P_2[k+n_1+n_2] \\ P_2[k+n_1+n_2-1] \\ -P_2[k-n_1-n_2-1] \\ P_2[k+n_2] \\ P_2[k+n_2-1] \\ P_2[k-n_2-1] \\ -P_2[k] \\ P_2[k-1] \end{bmatrix}^T \tag{4.19}$$

As before, the parameters are overdetermined in this system and are found similar to the LPM form: A_A can be found from the coefficients of $P_2(k+n_1+n_2)$, A_D can be found from the coefficients of $P_2(k)$, η_1 can be found from the coefficients of $P_2(k+n_1+n_2-1)$ and $P_2(k+n_1+n_2)$, and finally η_2 can be found from the coefficients of $P_2(k+n_1+n_2)$ and $-P_2(k-n_1-n_2-1)$.

An eigenvalue decomposition is also performed on the RPM model for each subject and intervention. Table 4.2 shows the mean and standard deviation of the eigenvalues and Figure 4.6 shows the mean associated eigenvectors. The exploration by the eigenvectors remains the same as the FPM.

Table 4.2: Eigenvalue Decomposition of RPM

Eigenvalues in Mean (SD)								
λ_1	λ_2	λ_3	λ_4	λ_5	λ_6	λ_7	λ_8	λ_9
0.28 (0.44)	1.05E6 (1.64E6)	1.70E6 (2.14E6)	2.74E6 (2.67E6)	1.23E8 (1.83E8)	4.13E8 (5.60E8)	1.84E9 (1.29E9)	4.23E9 (2.35E9)	7.70E9 (4.09E9)

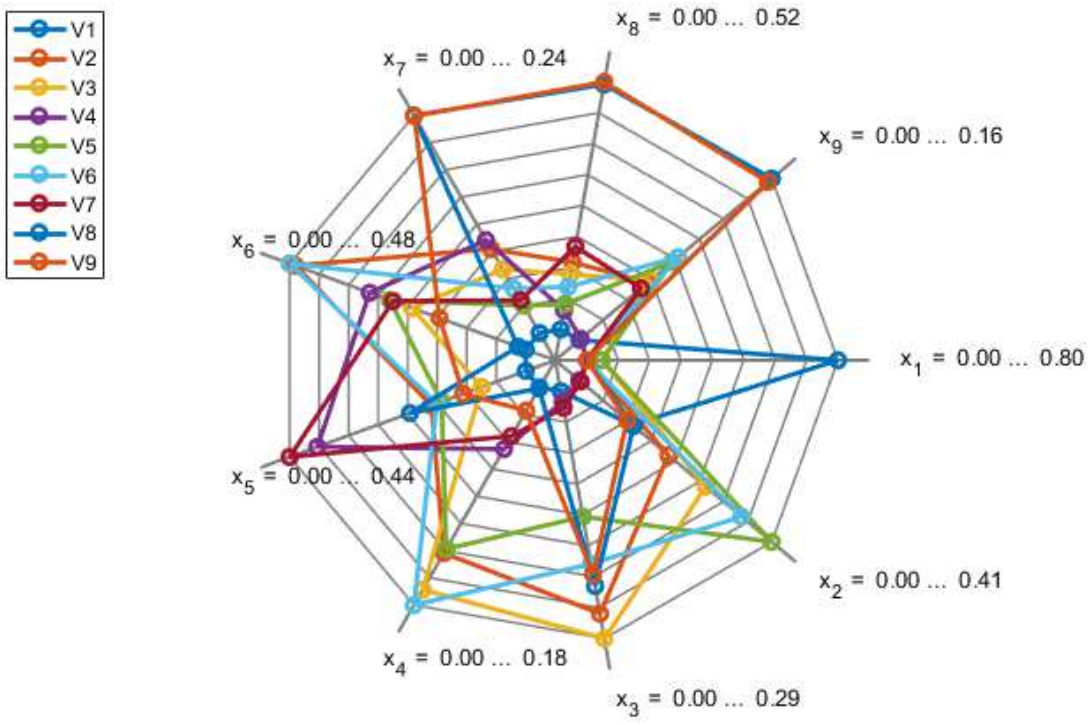

Figure 4.6: Eigenvectors for RPM Variant

4.2.2 Sensitivity Analysis

4.2.2.1 Data Sets

A quantitative sensitivity analysis on the base mechanism model was conducted. This analysis, since it was implemented on the original mechanism model, applies to both the RPM and FPM varients. Invasive aortic waveforms were obtained from 21 adult cardiac surgical patients under approval of the University of Alberta Health Research Ethics Board. Two collection sites existed: one near the aortic arch and the other at the femoral artery of each patient, providing the mech-

anism model P_1 and P_2 pressures, respectively. The ascending aorta waveform, P_0 was generated by implementing a 20ms time-offset from the aortic arch waveform (see [1] for more details). The data sets were collected at a sampling rate of 100Hz. Since this provided only a 10ms resolution, the data was upsampled to 1Kz for the purposes of the sensitivity analysis.

The sensitivity of calculated BCG waveforms with respect to aortic areas and time delays were determined for each patient. The following sections shall discuss the methods by which the sensitivity analysis was conducted and provide tabulated results for each model parameter.

4.2.2.2 I/J/K Sensitivity to Aortic Areas

The critical features of the BCG wave are captured in the timing and magnitude of the I/J/K peaks. Thus the sensitivity of each of those peaks to the parameters is of greatest interest to this study. The sensitivity demonstrated here are normalized against nominal values unless otherwise stated.

Referring to the original equation (Eq. 4.8), the BCG I peak occurs at a nominal time t_I. That is:

$$\bar{I} = -A_A(P_0(t_I) - P_1(t_I)) + A_D(P_1(t_I) - P_2(t_I)) \tag{4.20}$$

Differentiating this equation with respect to A_A and normalizing by $\bar{I}$ and $\bar{A}_A$, the

sensitivity of the I peak to the ascending aortic area can be expressed as:

$$\frac{\partial \bar{I}}{\partial A_A}\frac{\bar{A}_A}{\bar{I}} = \frac{\bar{A}_A(P_1(t_I) - P_0(t_I))}{A_A(P_1(t_I) - P_0(t_I)) + A_D(P_1(t_I) - P_2(t_I))} \tag{4.21}$$

The same procedure may be repeated for the sensitivity of the I peak to A_D to yield the following equation:

$$\frac{\partial \bar{I}}{\partial A_D}\frac{\bar{A}_D}{\bar{I}} = \frac{\bar{A}_D(P_1(t_I) - P_2(t_I))}{A_A(P_1(t_I) - P_0(t_I)) + A_D(P_1(t_I) - P_2(t_I))} \tag{4.22}$$

Continuing the same method, the sensitivity of both the J and K peaks can be formulated.

$$\bar{J} = -A_A(P_0(t_J) - P_1(t_J)) + A_D(P_1(t_J) - P_2(t_J)) \tag{4.23}$$

$$\frac{\partial \bar{J}}{\partial A_A}\frac{\bar{A}_A}{\bar{J}} = \frac{\bar{A}_A(P_1(t_J) - P_0(t_J)}{A_A(P_1(t_J) - P_0(t_J)) + A_D(P_1(t_J) - P_2(t_J))} \tag{4.24}$$

$$\frac{\partial \bar{J}}{\partial A_D}\frac{\bar{A}_D}{\bar{J}} = \frac{\bar{A}_A(P_1(t_J) - P_2(t_J)}{A_A(P_1(t_J) - P_0(t_J)) + A_D(P_1(t_J) - P_2(t_J))} \tag{4.25}$$

$$\bar{K} = -A_A(P_0(t_K) - P_1(t_K)) + A_D(P_1(t_K) - P_2(t_K)) \tag{4.26}$$

$$\frac{\partial \bar{K}}{\partial A_A}\frac{\bar{A}_A}{\bar{K}} = \frac{\bar{A}_A(P_1(t_K) - P_0(t_K)}{A_A(P_1(t_K) - P_0(t_K)) + A_D(P_1(t_K) - P_2(t_K))} \tag{4.27}$$

$$\frac{\partial \bar{K}}{\partial A_D}\frac{\bar{A}_D}{\bar{K}} = \frac{\bar{A}_D(P_1(t_K) - P_2(t_K)}{A_A(P_1(t_K) - P_0(t_K)) + A_D(P_1(t_K) - P_2(t_K))} \tag{4.28}$$

These relationships reveal that each of the I/J/K waves vary with respect to

changes in A_A through the change in the ascending tube pressures. That is, the magnitude of the ascending tube pressure difference at each of the I/J/K wave will determine the relative sensitivity of each to A_A. Conversely, each wave is sensitive to changes in A_D through the descending tube pressures at each wave.

From examination of Figure 4.2, it is expected that the I wave will be more sensitive to the changes in A_A than A_D since the magnitude of the pressure differences in the ascending tube is larger than the differences in the descending tube at the time of the I wave. For the J wave, it is expected that the sensitivity to A_A will be nearly negligible as compared to A_D. Again, this is a cause of the pressure difference in the descending tube being significantly larger in magnitude than the difference in the ascending tube at the time of the J wave. The case is the same for the K wave as with the J wave.

At this point, the sensitivity may be directly calculated from the patient data set to verify these expectations. The results of these calculations are shown in Table 4.3. These results verify the expectation that the ascending aortic area has the greatest impact on the amplitude of the I wave. If a 10% increase in the area is applied, then a mean 15.8% increase in the I wave amplitude would occur (in the negative, headward direction for the I wave). Whereas the same increase in the ascending aortic area would only achieve a mean 4.5% and 0.1% decrease in the J wave and K wave amplitudes respectively. In terms of the descending aortic area, the I wave amplitude is approximately 2.5 times less sensitive to changes as compared to the ascending area.

As expected the J and K wave amplitudes are approximately 3.2 and 100 times

Table 4.3: I/J/K Amplitude Sensitivity to Aortic Areas

BCG Wave	Average Subject A_A Sensitivity	Average Subject A_D Sensitivity
I Wave	1.58 ± 0.22	-0.58 ± 0.22
J Wave	-0.45 ± 0.46	1.45 ± 0.46
K Wave	-0.01 ± 0.31	1.01 ± 0.31

more sensitive to changes in the descending aortic area than the ascending area, respectively. However relative to each other, the J and K wave are comparably sensitive to changes in the descending aortic area, with the J wave slightly more sensitive. Thus the model-estimated descending area will depend simultaneously on the measured J and K waves.

It is assumed throughout this sensitivity analysis that the timing of the I/J/K waves remains constant despite area perturbations. To validate this assumption, timing changes in each of the I/J/K waves were measured after a large change (i.e., 20%) in aortic areas was applied. Table 4.4 shows the timing change of each wave was negligible despite these changes, thus validating the preceding analysis.

Table 4.4: I/J/K Timing Sensitivity to Aortic Areas

	Absolute Time Change (ms)			
BCG Wave	A_A + 20%	A_A - 20%	A_D + 20%	A_D - 20%
I Wave	-1.20 ± 3.32	2.40 ± 4.36	2.00 ± 4.08	-1.60 ± 4.73
J Wave	-1.20 ± 3.32	2.40 ± 2.40	2.40 ± 4.36	-1.60 ± 3.74
K Wave	0.40 ± 3.51	-1.20 ± 3.32	-0.80 ± 2.77	0.40 ± 3.51

With a large perturbation in the aortic areas, the change of the time occurrence of each wave is very small. For example, if the ascending area is changed by twenty percent, the time I wave has a mean change of 1.2 ms. The average time difference

between the BCG-I wave and BCG-J wave is 66ms whereas the average time delay between the BCG-I wave and BCG-K wave is 148ms. Thus a change in the I wave of 1.2ms is 1.8% of the I-J difference and 0.8% of the I-K difference. It can therefore be concluded that these absolute time changes are very small and each wave deemed to have low variability with respect to the aortic areas.

4.2.2.3 I/J/K Sensitivity to τ_1/τ_2

Sensitivity of each BCG wave relative to time-delay terms τ_1 and τ_2 was also studied. It is expected that a change in time-delay terms will result in larger variations in I/J/K wave timings. Thus a timing analysis was conducted prior to an amplitude study. A nominal value was available for τ_1 (i.e., 20ms), however no such value was defined for τ_2. To obtain this value, PTT was measured between P_1 and P_2 for each patient and τ_2 perturbations were based on this value (e.g., a time-delay between P_1 and P_2 of 60ms would be shifted $\pm$ 12ms for a 20% change). This timing analysis was conducted empirically as in the aortic area sensitivity analysis and the results are shown in Table 4.5

Table 4.5: I/J/K Timing Sensitivity to Time-Delays

	Absolute Time Change (ms)			
BCG Wave	τ_1 + 20%	τ_1 - 20%	τ_2 + 20%	τ_2 - 20%
I Wave	0.05 $\pm$ 0.38	0.38 $\pm$ 0.59	11.33 $\pm$ 5.26	-0.24 $\pm$ 0.77
J Wave	-0.57 $\pm$ 0.81	0.33 $\pm$ 0.58	3.90 $\pm$ 6.24	6.10 $\pm$ 3.66
K Wave	0.71 $\pm$ 0.90	0.14 $\pm$ 3.40	-2.33 $\pm$ 14.72	11.33 $\pm$ 9.33

The time-delay, τ_2, appears to be a significant factor in the timing of the BCG waves. The I and K wave appear to be the most sensitive to this aortic PTT.

Since the timing of the I/J/K waves change significantly for a change in τ_2, an amplitude sensitivity study as done for the aortic areas is unreasonable. However, the I/J/K wave have low variability with respect to τ_1 and so an amplitude sensitivity is conducted for this parameter.

The sensitivity equation for τ_1 was based on the fact that $P_0(t) = P_1(t + \tau_1)$. The normalized sensitivity is shown for the I wave, though the procedure is the same for the J and K waves.

$$\begin{aligned} \bar{I} &= -A_A(P_1(t_I + \tau_1) - P_1(t_I)) + A_D(P_1(t_I) - P_2(t_I)) \qquad (4.29) \\ \frac{\partial \bar{I}}{\partial \tau_1}\frac{\bar{\tau}_1}{\bar{I}} &= \frac{-P_1'(t_I + \tau_1)A_A\bar{\tau}_1}{A_A(P_1(t_I) - P_0(t_I)) + A_D(P_1(t_I) - P_2(t_I))} \end{aligned}$$

P_1' was evaluated numerically by a discrete forward difference method. Average results for individual patients are shown in Table 4.6.

Table 4.6: I/J/K Amplitude Sensitivity to τ_1

BCG Wave	Average Subject τ_1 Sensitivity
I Wave	1.77 ± 0.24
J Wave	-0.36 ± 0.41
K Wave	-0.08 ± 0.32

The BCG I wave is the most sensitive of the waves to the ascending aortic PTT. This supports the theory that the time delay between P_0 and P_1 has the greatest effect on the I wave (i.e., that the I wave occurs at the top of the aortic arch where P_1 is located). The results for the J wave amplitude show that it is inversely related to τ_1. This makes intuitive sense since, referring to Figure 4.2, the

J wave includes a small pressure difference between P_1 and P_0. An increased time-delay between these two parameters would result in a larger magnitude difference at the J wave location, lowering the overall magnitude of the J wave. In addition, this also follows previous assertions that the J wave occurs due to the movement of blood from the upper arteries to the lower arteries.

It is also interesting to note the K wave amplitude appears to have little to no dependence on the ascending aortic time delay. This also follows from Figure 4.2 since there is very little contribution from the ascending tube pressure difference. This result also agrees with previous theories that the K wave occurs at some point in descending arteries [35].

4.3 Methods

At this point, the model-based approach shall used to provide an estimation of BP via PTT and compare to these results to the signal-based approach. Data from the signal-based method provide a BP waveform as an input to the model (i.e., the Finapres BP). At noted previously, the location of the Finapres BP measurement was at the index finger of the subjects left hand. Thus the PTT estimated from this model-based method shall be compared to the Arm PTT from the previous study. This is inherently a limitation of the following analysis, since the mechanism of the BCG is due to descending arterial forces. This limitation is acknowledged and discussed in a later section.

Since there were beat exclusions conducted prior to selection of the five rep-

resentative intervention beats, there were many selected beats which were not continuous. That is, a set of five beats may initially have been a set of 6 beats with one removed due to a time-delay outlier. This model-based method requires the use of continuous data and thus all beats starting from two prior to the first beat of the originally identified five to two posterior to the last beat of the original five where used as input for each subject. Note that the addition of two beats before and after are required due to the SYSID technique (i.e., Equations 4.15 and 4.16 require some information prior to and after the current BCG estimation step). Only the five original beats were included in the cost function of the optimization technique to ensure a comparable result to the signal-based method. Figure 4.7 shows an example BP input with the corresponding measured BCG. The bolded BP beats denote the original five beats used in the signal-based method.

An estimate of the measured BCG wave is generated using both the FPM and the RPM techniques. The resulting estimated parameters from the model are critiqued for physiological reasonableness. Estimation of DBP and SBP is subsequently conducted as in the signal-based approach and results are compared.

4.3.1 Data Exclusion

The signal-based approach relied on only the BCG-I wave detection and not on the whole waveform. As such many of the beats used in the approach were not of the I/J/K form. That is, some beats exhibited double peaks in either I, J, or K, while other beats had a significant slope change in either the I/J upstroke or the

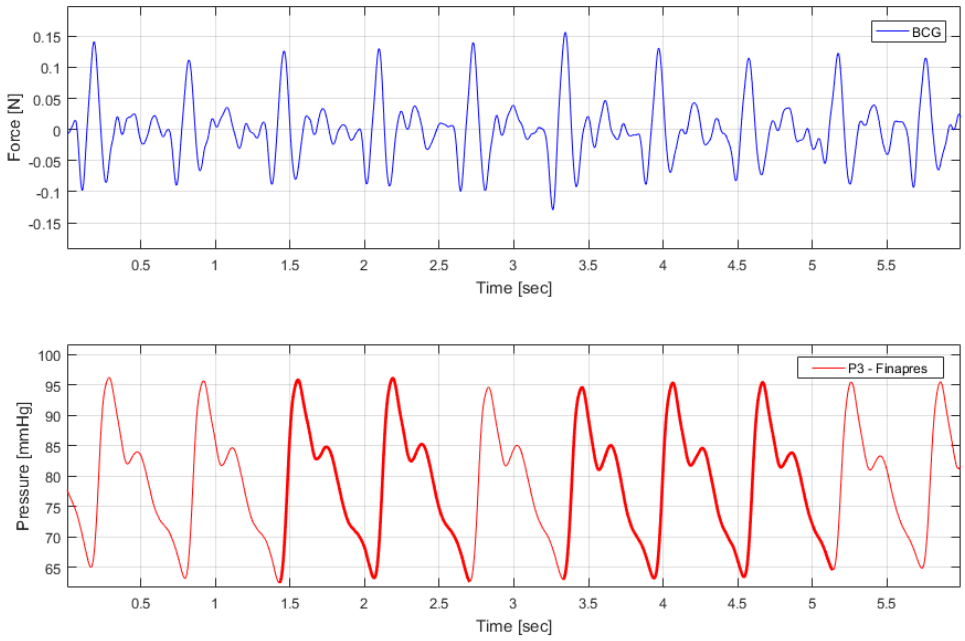

Figure 4.7: An example of input BP and corresponding BCG. Bolded beats show those used from the weighing-scale study. Un-bolded beats are included for data continuity and adequate input data for transmission line theory estimation.

J/K downstroke. Examples of these waveforms compared to a reasonable BCG are shown in Figure 4.8.

It is unreasonable at this time to expect the BCG model to estimate these types of waves since the model was originally developed to show key BCG characteristics. Thus, for the purposes of first validating the model as it is currently intended, beats were excluded from estimation of subject PTT. The model-based approach shall examine 8 subjects (subject numbers 2, 3, 4, 5, 6, 10, 11, and 17 from Table 3.1) which had 50% or more reasonable beats and no more than 1 excluded intervention (an intervention is excluded due to no usable beats). Data that are excluded at this

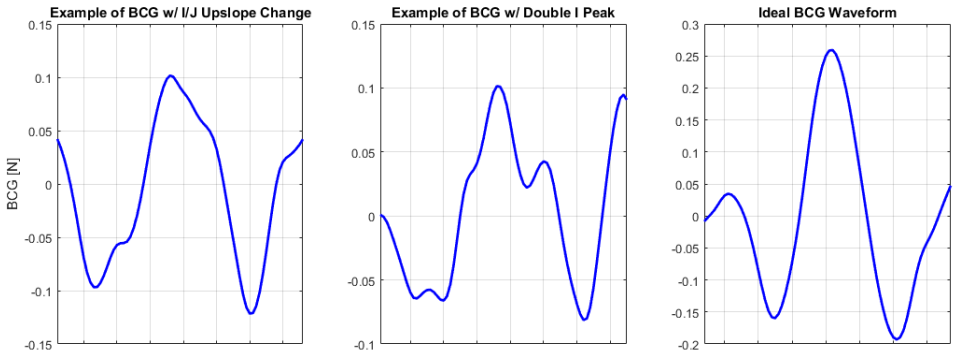

Figure 4.8: Examples of measured BCG waveforms taken from a single subject within the same intervention. The leftmost figure exemplifies a change in I/J upstroke slope. The middle figure shows both a double I peak and a change in the J/K downstroke. The rightmost figure shows the expected waveform of the mechanism model.

time should be examined when improving the model, however that is beyond the scope of this thesis.

4.3.2 Data Limitations

There are certain limitations of the data set used for this thesis which must be acknowledged. Firstly, the Finapres BP waveform is measured from a radial artery and not a descending artery. Since the genesis of the BCG is attributed to descending pressures, the original model was based off of this attribute. However, it is not wholly unreasonable to apply the radial Finapres BP to this model due to similarities in femoral (descending) and radial BP waveforms. Figure 4.9 shows an example of a femoral and radial BP waveform measured from the same subject.

While the femoral waveform has a greater pulse pressure (PP) than the radial

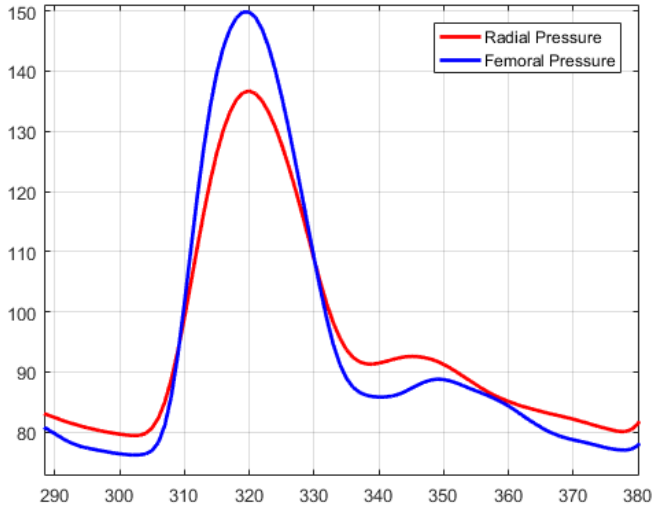

Figure 4.9: An example of radial and femoral BP waveforms measured invasively from [1]

waveform, the waveform features are very similar. The timing of the diastolic and systolic pressures are similar. Thus arm PTT estimation is expected to be reasonable with this model. Also, the overall morphology of each wave is similar, each exhibiting the a "diacrotic notch" near the same time (note this is not the true diacrotic notch known to occur at the ascending aortic pressure, but is the transmission of this occurance through the arterial tree). Thus with similar morphology and timing, it is reasonable to use a radial waveform instead of the femoral waveform for estimation of arm PTT.

Another limitation of this data is there are no measured intermediate pressures, resulting in blind identification of intermediate pressures for BCG estimation. This may result in non-physiological intermediate pressures since there is no training data for the intermediate pressures. Future studies should include the measurement of

intermediate waveforms for full validation of estimated parameters.

4.3.3 Optimization Techniques

Both the RPM and FPM were optimized in the same way (i.e., only the calculation of the estimated BCG wave differed, not the cost function formulation). The cost function along with its constraints are provided below and discussed in the remainder of this section.

$$\text{Minimize} \quad f(A_A, A_D, \eta_1, \eta_2) = \sqrt{\frac{1}{n}\sum (BCG_{measured} - BCG_{estimated})^2}$$

$$\text{subject to} \quad g_1 = -A_A < 0$$

$$g_2 = -A_D < 0$$

$$g_3 = -\eta_1 + 0.01 < 0$$

$$g_4 = -\eta_2 + 0.01 < 0$$

$$g_5 = -\eta_1 + 1.02\eta_2 < 0$$

$$g_6 = -A_A + A_D < 0$$

$$g_7 = \eta_1 + \eta_2 - 1.8F_s < 0$$

$$g_8 = A_A - 0.0007 < 0$$

This optimization is applied to each beat, providing a beat-specific set of estimated parameters for each intervention. In addition, since PTT is the most im-

portant parameter for estimation, this optimization is performed on all physiological combinations of τ_1, τ_2, and τ_3. That is, values for τ_1, τ_2, and τ_3 were set prior to the optimization according to physiological bounds and iterated through a range of values, performing the optimization on each set. This procedure yielded many hundreds of minimized cost function values and the final estimated parameters are chosen by selecting the set which corresponded to the smallest cost function value. Due to the large number of optimizations, the data was down-sampled to a 200Hz, providing 2ms of PTT resolution.

The cost function, f, is simply the RMSE of the estimated BCG and the measured BCG. The cost function only takes into account the time range which includes the I/J/K waves of each beat of the measured BCG since these are the major features of the wave. The estimated BCG is calculated for a single beat from the discrete functions given in Equations 4.15 and 4.16 for the FPM and RPM respectively.

The constraints applied to this function stem from physiological restrictions. The need for g_1 and g_2 is clear since aortic areas cannot be negative. In addition, to ensure appropriate reflection coefficients, constraints g_3 - g_5 are used to ensure η_1/η_2 take values sufficiently far away from zero (preventing both infinite and zero reflection coefficients) and that they are sufficiently distinct from each other (prohibiting a reflection coefficient near one which would result in a simple time-delay between waves). Also, g_6 requires A_A to be larger than A_D since aortic areas decrease as the artery is further away from the heart. g_7 places an upper bound based on the sampling frequency F_s on η_1/η_2 values to ensure sufficient distance from the Nyquist

frequency. Finally, g_8 is based from measured values of ascending aortic area [33]. This is to ensure A_A does not become larger than physiologically reported values.

The optimization was performed with MATLAB's fmincon function using the default "interior-point" method. As previously noted, the optimization was run for all physiologically reasonable combinations of τ_1, τ_2, and τ_3. The ranges for these parameters was determined from boundaries on pressure timings described earlier. For the FPM, τ_3 was assumed to be a small value between -30ms to 30ms, including zero. This choice was justified by measuring the time difference between the Finapres SBP and the measured BCG K peak for each beat. It was found that 89.5% of the used beats remained within this range. In the RPM case, τ_3 was set to equal the time difference between the Finapres SBP and the BCG K wave.

In regards to the physiological bounds on τ_2 and τ_1, the diastole of P_1 occurs at some point between the BCG I peak and the H peak. Thus the search range of τ_2 started from the difference between the time of measured Finapres DBP and measured I wave (minus the current value of τ_3) and ended at the time difference between the measured Finapres DBP and measured H wave (minus the current value of τ_3). This was the case for both the FPM and the RPM. Similarly, P_0 occurs at some point after the BCG H wave. Thus the start of the search range for P_0 was the time difference between Finapres DBP and BCG I wave (minus both τ_2 and τ_3) and the ended at the time difference between Finapres DBP and BCG H wave (minus both τ_2 and τ_3).

4.4 Results

4.4.1 PTT Selection

Through the application of the model-based approach, it was found that the most accurate PTT estimation came through the sum of τ_2 and τ_3. This is due to the range of acceptable values for the sum of all estimated PTT values (i.e., τ_1, τ_2, and τ_3). This range has a maximum value of the time difference between the measured DBP and the measured BCG-H wave. As previously mentioned, the BCG-H wave is known to occur sometime prior to left ventricular ejection, and so it is possible for this PTT to include some portion of PEP. Examining Figure 4.2, the diastolic of P_1 is at some point between the modeled I wave and H wave, near the occurrence of left ventricular ejection. Thus, any inclusion of PEP in the model-based PTT would be in time-delay between P_1 and P_0, τ_1. Thus all model-based results discussed henceforth shall refer to estimated PTT as the sum of τ_2 and τ_3 only.

4.4.2 FPM Results

Figure 4.10 shows a typical estimated BCG waveform from the FPM. This varient was able to accurately estimate the I/J/K waves of the BCG, estimated amplitude and time results are provided later. Table 4.7 summarizes the model-estimated parameters for each subject and intervention. Interventions noted as excluded are due to no usable BCG waveforms from the original study in [36]. In addition, some interventions had only one usable beat out of the five provided,

thus standard deviation is not applicable to that intervention. In each subject, the

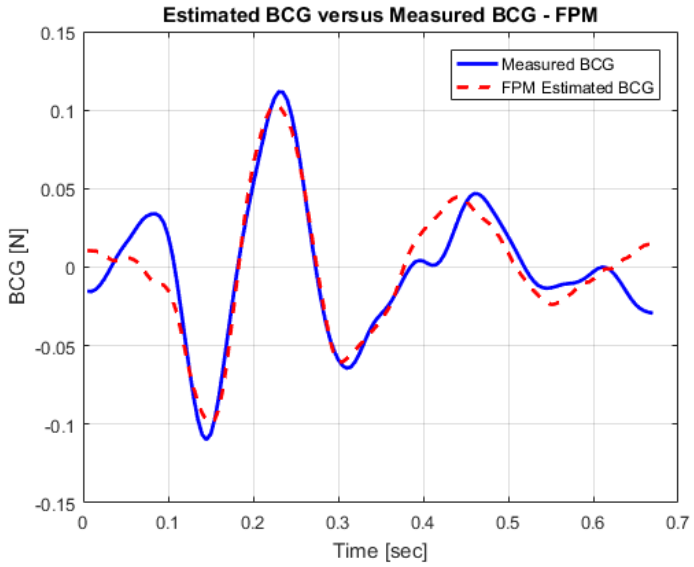

Figure 4.10: An example of a typical FPM estimated BCG

following observations can be made regarding the results. First, the estimated PTT has the desired trend in relation to DBP in most of the subjects. That is, each intervention period results in a higher DBP relative to the previous resting period. Since PTT is known to have an inverse relationship to changes in DBP, it would be expected that each intervention has a lower PTT as compared to the previous resting section. This is true for the estimated PTT.

In addition, the ascending aortic area is expected to be between 7.00e-4 m^2 and 7.06e-5 m^2 (population average left subclavian aortic area) [33]. In 9% of the interventions, the mean area is slightly lower than the expected lower bound. These ascending area results are still acceptable however since the reference areas are population averaged and some deviation from these values is acceptable.

Table 4.7: FPM Results

		Mean Estimated Paramaters					DBP
Subject	Interv.	PTT (ms)	A_A (m^2)	A_D (m^2)	η_1	η_2	(mmHg)
2	R1	70±9	6.68E-05	5.89E-05	167.34	108.13	58.77
	MA	58±4	5.21E-05	5.21E-05	43.10	33.62	99.15
	R2	83±16	2.06E-04	6.04E-05	100.41	73.46	57.66
	CP	73±13	1.24E-04	4.88E-05	88.21	63.19	86.67
	R3	78±13	2.85E-04	5.83E-05	166.17	108.31	59.66
	PE	65 (N/A)	5.14E-05	4.67E-05	198.91	157.82	91.64
3	R1	78±3	5.19E-04	7.19E-05	100.12	50.51	64.77
	MA	71±6	6.17E-04	7.82E-05	93.39	77.62	81.84
	R2	77±8	2.56E-04	6.15E-05	17.59	13.24	65.07
	CP	63±11	1.37E-04	7.41E-05	188.09	129.47	76.37
	R3	86±6	3.06E-04	9.24E-05	67.96	38.83	60.68
	PE	74±12	5.02E-04	1.18E-04	76.07	41.72	61.53
4	R1	105±11	5.79E-04	8.32E-05	58.42	32.15	76.65
	MA	93±9	2.56E-04	7.72E-05	156.03	91.29	103.27
	R2	99±7	3.32E-04	9.20E-05	82.78	44.61	72.51
	CP	103±11	2.23E-04	5.73E-05	155.11	84.24	87.21
	R3	101±17	4.62E-04	8.24E-05	15.56	14.99	69.41

Continued on next page

Table 4.7 – *Continued from previous page*

Subject	Interv.	PTT (ms)	A_A (m^2)	A_D (m^2)	η_1	η_2	DBP
	PE	83±10	2.04E-04	8.50E-05	220.02	111.15	92.05
5	R1	89±9	1.47E-04	7.98E-05	61.22	45.00	81.87
	MA	88±6	3.27E-04	8.77E-05	47.59	28.51	96.15
	R2	97±10	4.86E-04	1.07E-04	41.43	33.98	81.75
	CP	80±4	5.49E-04	1.02E-04	81.75	57.60	112.34
	R3	97±8	3.91E-04	7.98E-05	31.23	23.13	81.24
	PE	73±12	1.19E-04	6.86E-05	142.65	128.84	104.93
6	R1	100±10	6.86E-05	1.32E-04	148.56	99.92	75.32
	MA	Intervention Excluded					
	R2	86±2	2.46E-04	2.21E-04	96.18	68.63	73.62
	CP	95±14	5.19E-04	7.44E-05	100.07	58.07	83.35
	R3	99±15	3.06E-04	1.55E-04	192.12	106.64	68.44
	PE	73±10	2.46E-04	1.10E-04	23.82	13.50	90.84
10	R1	87±6	4.25E-04	1.61E-04	91.99	76.35	68.07
	MA	75±14	4.33E-04	1.74E-04	100.07	97.92	79.23
	R2	87±10	5.14E-04	1.58E-04	42.92	33.56	61.22
	CP	78±11	4.49E-04	4.01E-04	59.16	57.72	66.16
	R3	100±0	4.39E-04	1.26E-04	86.66	60.88	64.15
	PE	Intervention Excluded					

Continued on next page

Table 4.7 – *Continued from previous page*

Subject	Interv.	PTT (ms)	A_A (m^2)	A_D (m^2)	η_1	η_2	DBP
11	R1	95±9	4.64E-04	6.97E-05	34.76	20.59	79.01
	MA	75±21	3.37E-04	7.33E-05	60.32	40.73	89.70
	R2	91±9	3.68E-04	7.34E-05	80.00	56.39	75.94
	CP	Intervention Excluded					
	R3	73±3	2.34E-04	8.82E-05	130.25	100.56	74.71
	PE	60 (N/A)	7.58E-05	7.58E-05	256.02	102.56	86.59
17	R1	88±6	1.05E-04	9.00E-05	65.57	25.94	78.11
	MA	70 (N/A)	9.35E-05	8.24E-05	96.60	79.27	109.59
	R2	84±14	2.34E-04	9.07E-05	122.18	116.44	91.95
	CP	78±15	4.39E-04	1.06E-04	80.13	65.07	97.70
	R3	75±9	1.69E-04	9.57E-05	130.20	95.79	90.50
	PE	Intervention Excluded					

A similar analysis of the descending area can be made. The upper bound of the descending area is determined by the identified ascending area, however a reasonable lower bound would be that of the population average left interosseous artery (9.29e-6 m^2 [33]). All of the mean estimated decending areas fall above this lower bound and thus these estimated areas are deemed physiologically reasonable. (Note: without comparison against patient-specific data, this is the only assertion about the validity of the areas that can be made at this time).

It is much more difficult to determine the validity of the reflection coefficient parameters, η_1 and η_2. In fact, without an intermediate BP waveform to examine these parameters against (i.e., comparing an intermediate pressure generated by these parameters with a measured waveform) it is impossible to make any definitive conclusions. Some reference values are provided in [47] where invasive measured radial waveforms were transformed by a lossy tube load model with a 3-element windkessel load to central aortic BP waveforms. The values reported from that study are 33.4 ± 31.7 and 12.6 ± 11.4 for η_1 and η_2 respectively. Values identified in this model are significantly larger than previously reported and further investigation into this aspect of the model is required.

The next section shall present the results from the RPM model, followed by a comparison of the two models to signal-based arm PTT.

4.4.3 RPM Results

Figure 4.11 shows a typical estimated BCG waveform from the RPM. The model was able to estimate the magnitude of the I/J waves of the BCG with some difficultly in estimating the K wave and the J wave timing. More discussion on this shortcoming is provided below. Table 4.8 summarizes the model-estimated parameters for each subject and intervention. The results shown in Table 4.8 are similar to those from the FPM. The inverse trend between PTT and BP is maintained in most subjects in this model. However, in some interventions, the estimated change in PTT is either in the wrong direction or zero thus causing overall correlations to

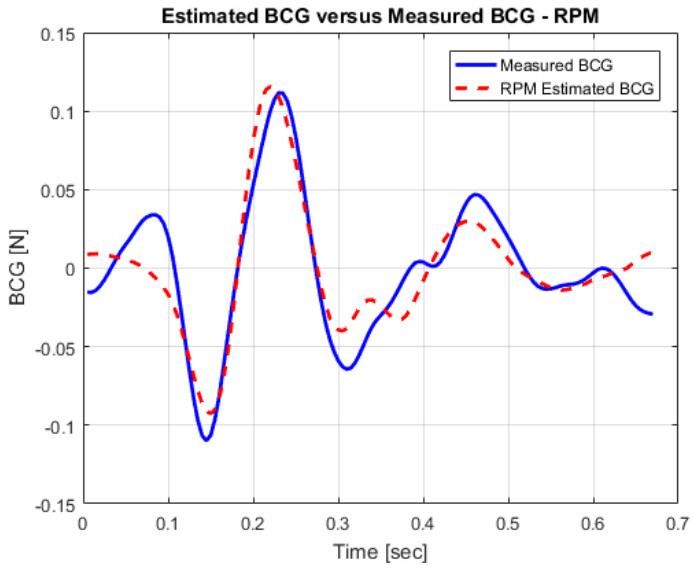

Figure 4.11: An example of a typical RPM estimated BCG

be reduced (See the next section for a discussion on correlations). The majority of estimated values of A_A fall within the expected range with only 7% occurring outside. Estimated A_D values are also physiologically reasonable with all of the predicted values larger than the popuation average left interosseous artery area. Estimated values for η_1 and η_2 appear to be significantly more reasonable than the FPM. Comparing to the values reported in [47], 66% of the values determined for η_1 fall within a single standard deviation of the reported values and 80% fall within two standard deviations of the mean. However, only 50% of the values for η_2 fall within one standard deviation of the reported mean and 64% are within two standard deviations. Even though this analysis for η_1 and η_2 is not quantitatively thorough, the RPM does appear to result in more reasonable parameters than the FPM.

Table 4.8: RPM Results

		Mean Estimated Paramaters					DBP
Subject	Interv.	PTT (ms)	A_A (m^2)	A_D (m^2)	η_1	η_2	(mmHg)
2	R1	68±12	7.00E-05	6.84E-05	10.75	7.61	58.77
	MA	68±4	7.02E-05	5.67E-05	19.76	1.56	99.15
	R2	71±17	1.00E-04	9.26E-05	7.84	7.68	57.66
	CP	69±13	1.58E-04	7.64E-05	10.07	9.74	86.67
	R3	69±13	1.00E-04	5.85E-05	12.24	9.12	59.87
	PE	65 (N/A)	5.27E-05	4.86E-05	122.52	86.49	91.64
3	R1	78±3	4.30E-04	6.79E-05	124.27	74.07	64.77
	MA	69±5	3.46E-04	7.09E-05	55.62	45.09	81.84
	R2	80±10	8.23E-04	1.01E-04	85.28	74.52	65.13
	CP	58±18	1.24E-04	7.26E-05	107.11	72.83	76.37
	R3	86±11	3.33E-04	8.67E-05	112.45	73.92	60.68
	PE	77±10	7.37E-04	1.17E-04	97.29	68.84	61.53
4	R1	104±11	5.38E-04	7.52E-05	30.5	21.36	76.6
	MA	89±3	2.09E-04	6.90E-05	108.49	83.46	103.3
	R2	97±4	2.93E-04	8.48E-05	15.97	10.81	72.5
	CP	103±10	3.00E-04	5.26E-05	135.54	91.90	87.2
	R3	100±18	4.40E-04	8.55E-05	10.90	10.68	69.4

Continued on next page

Table 4.8 – *Continued from previous page*

Subject	Interv.	PTT (ms)	A_A (m^2)	A_D (m^2)	η_1	η_2	DBP
	PE	82±8	1.61E-04	8.28E-05	223.51	126.47	92.1
5	R1	90±9	1.59E-04	7.03E-05	79.28	46.83	81.9
	MA	90±5	5.58E-04	8.96E-05	69.32	42.42	96.1
	R2	95±9	2.80E-04	9.86E-05	26.91	23.20	81.7
	CP	83±6	7.77E-04	9.31E-05	24.04	19.86	112.3
	R3	101±13	3.44E-04	5.67E-05	32.29	27.52	81.2
	PE	71±9	9.49E-05	5.81E-05	45.32	44.20	104.9
6	R1	96±8	2.42E-04	1.17E-04	14.06	12.05	75.3
	MA	Intervention Excluded					
	R2	91±7	2.66E-04	2.04E-04	85.14	50.06	73.5
	CP	93±18	5.17E-04	7.06E-05	60.24	31.49	83.5
	R3	103±16	2.64E-04	1.17E-04	66.44	37.23	68.4
	PE	73±10	3.42E-04	1.14E-04	31.99	16.88	90.8
10	R1	88±13	8.23E-04	1.53E-04	17.11	15.07	65.25
	MA	78±11	4.15E-04	2.48E-04	96.53	30.67	79.23
	R2	87±16	4.62E-04	1.51E-04	25.28	20.69	61.22
	CP	88±4	6.98E-04	6.27E-04	7.59	6.51	66.16
	R3	95±7	5.99E-04	1.27E-04	18.24	13.47	64.15
	PE	Intervention Excluded					

Continued on next page

Table 4.8 – *Continued from previous page*

Subject	Interv.	PTT (ms)	A_A (m^2)	A_D (m^2)	η_1	η_2	DBP
11	R1	95±9	4.93E-04	7.31E-05	36.89	22.01	79.01
	MA	73±22	3.09E-04	7.45E-05	11.53	11.06	89.70
	R2	85±4	2.44E-04	7.60E-05	25.50	18.01	75.94
	CP	Intervention Excluded					
	R3	70±9	2.79E-04	7.50E-05	12.98	11.00	74.71
	PE	65 (N/A)	9.15E-05	7.64E-05	278.28	80.71	86.59
17	R1	92±6	1.27E-04	8.50E-05	94.87	34.61	78.11
	MA	70 (N/A)	8.57E-05	8.38E-05	46.26	31.86	109.59
	R2	84±15	1.89E-04	7.95E-05	38.94	26.43	91.95
	CP	72±10	2.28E-04	1.30E-04	15.57	11.12	97.70
	R3	70±9	1.14E-04	8.23E-05	20.11	14.32	90.50
	PE	Intervention Excluded					

4.4.4 Accuracy of FPM and RPM

The accuracy of each model is quantitatively evaluated in terms of both amplitude error and timing error of each wave. Both of these errors was evaluated for the I/J/K waves in each of the FPM and RPM and reported in terms of mean and standard error of RMSE in Table 4.9. RMSE was computed for each intervention for each subject, resulting in 44 values. Overall prediction accuray of the I wave

was very similar in terms of both amplitude and timing. However the FPM outperforms the RPM in the J and K waves for both timing and amplitude. This is expected since the RPM sets the value for τ_3 which determines the position of the distal pressure for the mechanism model. Since the distal pressure plays a large role in determining the J and K waves (See figure 4.2), inaccuracy will be introduced by this method.

Table 4.9: RMSE of FPM and RPM. Results shown in terms of mean and standard error

	Wave Amplitudes RMSE [N]			Wave Timing RMSE [ms]		
Model	I Amp	J Amp	K Amp	I Time	J Time	K Time
FPM	0.018 (0.002)	0.014 (0.002)	0.020 (0.004)	5.2 (0.4)	5.7 (0.4)	6.5 (0.5)
RPM	0.021 (0.002)	0.023 (0.002)	0.31 (0.003)	6.4 (0.8)	8.7 (0.8)	10.9 (1.7)

A paired T-test was used to assess the significance of the mean differences. It was found that for all J and K amplitude and timing results, the means were statistically different ($p < 0.05$) according to the two-tail test. However the results for the I wave amplitude and timing were not statistically significant ($p = 0.23$ & $p = 0.18$, respectively). Thus the FPM variant is indeed more accurate than the RPM in J and K waves.

The following sections will compare the FPM and RPM results to those from the signal-based method and discuss intermediate results of each model (i.e., predicted pressures).

4.4.5 Comparison to Signal-Based Approach

Prediction of BP was calculated by taking the estimated PTT values and measured BP and performing a linear regression. The linear regression was then used to generate predicted BP values based on the estimated PTT. Figures 4.12 and 4.13 compare FPM and RPM predicted BP values respectively to measured BP. Pearson's linear correlation coefficients between model-based PTT and measured BP are reported in Table 4.10 for both models.

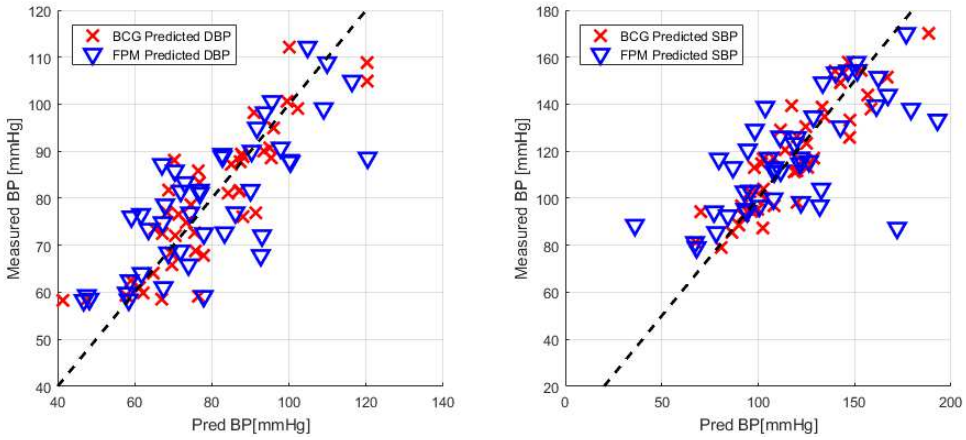

Figure 4.12: FPM predicted BP vs. BCG-I wave predicted BP

Correlations to BP are comparable to those previously obtained by the signal-based method. The FPM slightly outperforms the RPM in terms of mean and standard deviation correlation to DBP. Both models have poorer performance in SBP and the RPM slightly outperforms the FPM in this case. However a paired T-test showed that results in the FPM and RPM for both DBP and SBP are not significantly different from each other. The sensitivity of the FPM and RPM in BP

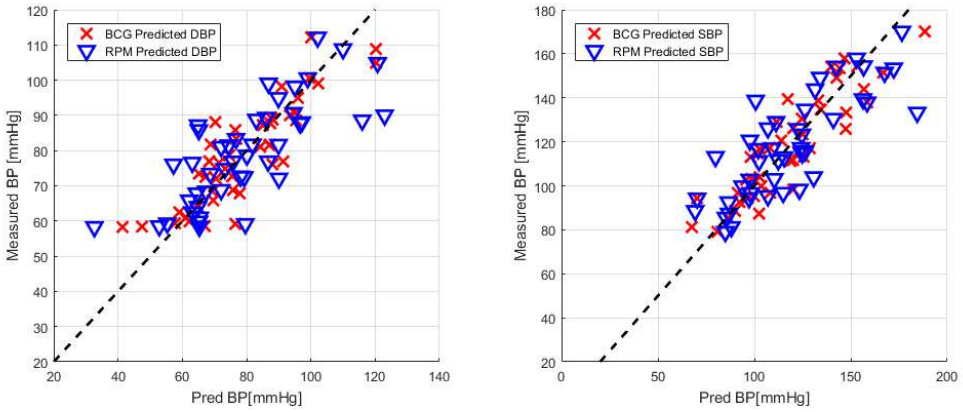

Figure 4.13: RPM predicted BP vs. BCG-I wave predicted BP

prediction is higher than that of the signal-based method showing that improvement in robustness against subject variations is needed. When compared to the signal-based method in both DBP and SBP prediction, the FPM and RPM could not be shown to be statistically different from the signal-based method by a paired T-test. In sum, the FPM and RPM predicted PTTs can be deemed reasonable due to the overall good BCG fitting and the comparable correlations to BP. Improvement is needed if this model is to be used as a replacement of previous techniques, however these first iteration results are promising for future applicability.

Both of the FPM and RPM variants outperform ECG-based PAT overall. While these outperformed PAT in half of the subjects for DBP, the sensitivity of this prediction is significantly less overall. In terms of SBP, the RPM continued to outperform PAT in half of the subjects while the FPM performed better in 3/8 subjects. However, the consistency of each model continues to be drastically improved in the FPM and RPM variants as compared to PAT. Thus the FPM and

Table 4.10: Correlation to BP. S.B. PTT refers to signal-based PTT and is corrected for the new DBP and SBP found after beat exclusion. Conventional PAT is also given for corrected DBP and SBP values after beat exclusion.

	Correlation to DBP				Correlation to SBP			
Subject	FPM	RPM	S.B. PTT	PAT	FPM	RPM	S.B. PTT	PAT
1	-0.81	-0.53	-0.84	-0.60	-0.78	-0.80	-0.83	-0.83
2	-0.72	-0.80	-0.88	-0.10	-0.84	-0.85	-0.87	-0.22
3	-0.61	-0.63	-0.93	-0.75	-0.50	-0.53	-0.89	-0.65
4	-0.86	-0.79	-0.78	-0.64	-0.90	-0.84	-0.83	-0.73
5	-0.72	-0.89	-0.87	-0.76	-0.50	-0.74	-0.88	-0.58
6	-0.63	-0.81	-0.62	-0.83	-0.36	-0.65	-0.50	-0.80
7	-0.53	-0.42	-0.77	-0.71	-0.65	-0.47	-0.84	-0.93
8	-0.87	-0.78	-0.65	0.14	-0.80	-0.70	-0.69	0.07
Mean	**-0.72**	**-0.71**	**-0.79**	**-0.53**	**-0.67**	**-0.70**	**-0.79**	**-0.58**
SD	**0.12**	**0.16**	**0.11**	**0.35**	**0.20**	**0.14**	**0.13**	**0.34**

RPM variants are overall improvements to the current PAT methods with need for improvement patient-specific results. Methods for these improvements are discussed in the future work section at the end of this chapter.

4.4.6 Intermediate Results - FPM and RPM

It is critical to examine not only the end BCG fitting and resulting model parameters, but the estimation of the intermediate pressures (i.e., P_1 and P_0) for physiological reasonableness. Figure 4.14 shows two examples of these pressures for each the FPM and RPM. Figures 4.14(c) & 4.14(d) show examples of reasonably estimated pressures while Figures 4.14(a) & 4.14(b) show examples of unreasonable pressures. It is physiologically unreasonable to have a "second systolic" pressure which is higher than the first (As seen in Figure 4.14(a)). Since all of the subjects in this study were healthy young adults with no history of cardiac illnesses, all

resulting pressures should have a reasonable waveform morphology. In addition, it is not reasonable to have a systolic peak larger in P_0 than in P_1 (Figures 4.14(a) & 4.14(b)).

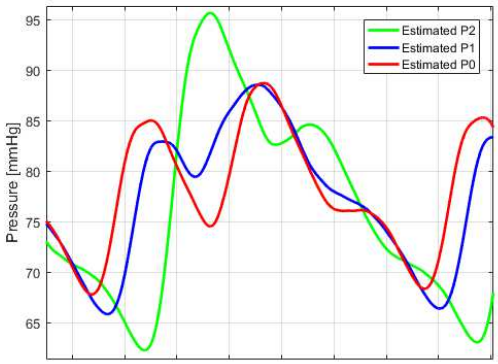

(a) FPM: Poor Pressure Estimation

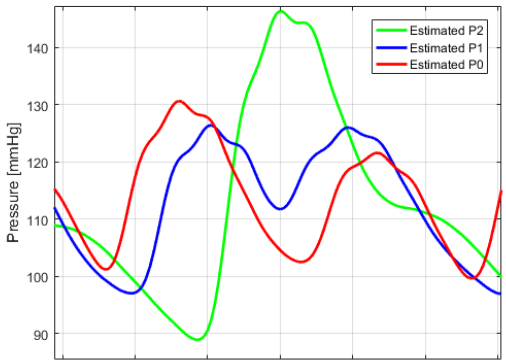

(b) RPM: Poor Pressure Estimation

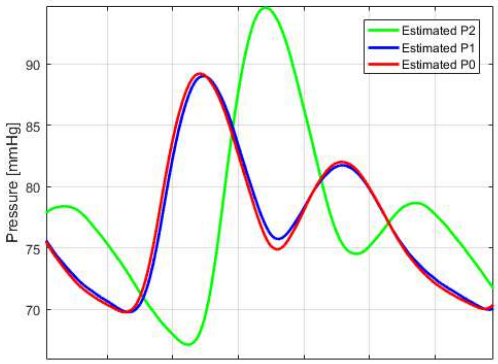

(c) FPM: Good Pressure Estimation

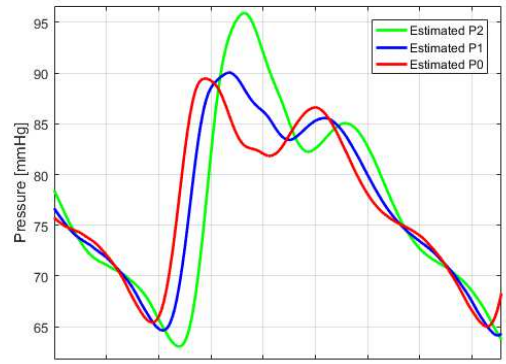

(d) RPM: Good Pressure Estimation

Figure 4.14: Examples of Intermediate Pressures from FPM and RPM

In both models, over half of the estimated waveforms for P_1 and P_0 were physiologically unreasonable (i.e., exhibited a "second systolic" pressure or had a larger PP in P_0 than in P_1). This is a large shortcoming of both of these models and is due to large pulse transit times. The foundation of transmission line theory is the segregation of pressure into the sum of forward and backward traveling waves.

These forward and backward waves are estimated at the distal site and shifted apart as the location of estimated pressure becomes more proximal (See Figure 4.15). If the forward and backward waves are shifted beyond a certain point, the peak of each of these waves will begin to be exhibited in the final estimated pressure. In addition, transmission line theory assumes zero mean pressure, thus each of the forward and backward waves will have a negative diastolic pressure. If shifting continues even further, the backward wave can, in some cases, decrease the peak from the forward wave resulting in a lower first peak.

4.4.7 Future Work

While the FPM and RPM variants have shown promise for model-based PTT estimation, it is clear that improvements are necessary. The first improvement area is the issue of intermediate pressure estimation. Addressing the assumptions of the tube-load model would be the first approach. Specifically, tube-load models assume non-interacting wave reflections. Typically this assumption is considered justifiable due to the fact that arterial termination sites constitute the highest impedance mismatch [45]. However in a blind-identification of pressures, such as is with this model, estimation of the true impedance mismatch is extremely difficult to achieve. Thus, a training pressure waveform may be necessary. That is, identification of patient-specific reflection coefficients by first estimating a measured central pressure (e.g., ascending aortic pressure) by a measured distal pressure followed by estimation of the patients BCG with the identified parameters. This is highly undesirable in the

case of ubiquitous monitoring since measurement of the central pressure is difficult to obtain. However, without such validation, it may be nearly impossible to further develop the BCG-based estimation of PTT.

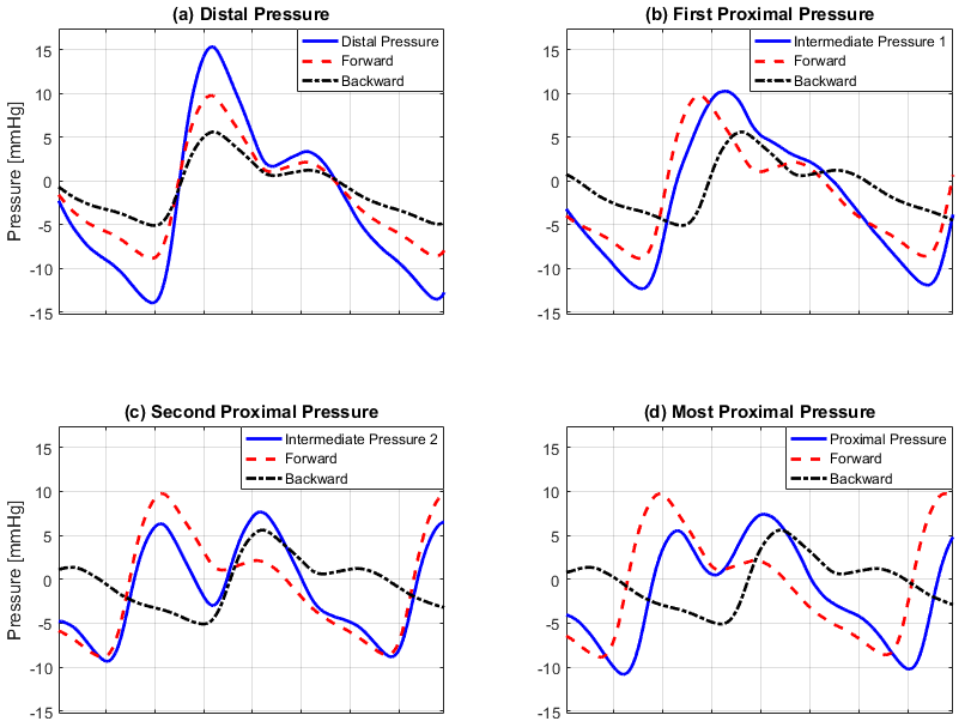

Figure 4.15: Transmission line theory forward and backward waves. (a) Forward and backward waves of the measured distal pressure. (b) An estimated proximal pressure showing separation of forward and backward waves. (c) A second proximal pressure with further separation exhibiting "double systole" peaks. (d) The most proximal pressure with the largest separation between forward and backward waves showing a "first systole" peak smaller than the second.

A second approach would be examining the assumption of a lossless tube-load model which may be too simplistic. Since tube lengths in this model are significant (i.e., over 60 cm), BP losses may be too great. This adds another layer of complexity

to the current model, in fact introduces two additional parameters which must be estimated (one additional parameter for the wave propagation coefficient and one for wave reflection coefficient). However it may be necessary to increase the complexity in order to reflect true physiological conditions.

Yet another area for improvement is determining the cause for lower correlations in certain subjects in both the FPM and RPM. Ways in which this may be accomplished are examining the measured BCG features for abnormalities not anticipated by the model. Specifically, the time difference between the I and J peaks as well as the I to K peaks may illuminate unusual BCG waves. Should the time delay between these peaks be abnormal within an intervention or certain number of beats, the estimated PTT would be larger or smaller depending on the deviation direction. If a relationship between certain abnormalities and lower BP prediction correlations be found, then the model can be improved to provide robustness against these abnormalities.

As previously discussed, a limitation of this model is the lack of verification against descending aortic waveforms. Since the BCG originates from descending aortic events, the use of radial waveforms is a limiting factor in this thesis. Future work should examine the application of this model to waveforms consistent with the mechanism of the BCG.

Chapter 5: Conclusion

In conclusion, a BCG-based approach to PTT estimation has been described. Two approaches were studied. The signal-based approach studied the efficacy of a BCG-based PTT over current ECG-based PAT methods. It was found that BCG-based PTT was more robust than ECG-based PAT due to the inclusion of PEP and arm PTT in PAT.

Exploration of BCG-based PTT was further studied through the development of a model-based approach. This approach consisted of two varients, one which estimated all PTT parameters and the other which determined one of the PTT parameters by physiological measurements, were presented. Both models showed comparable results to signal-based PTT techniques and facilitated the identification of intermediate parameters. Some of these parameters, (i.e., aortic areas) were deemed to be physiologically reasonable, while others (i.e., reflection coefficient parameters) were shown to be reasonable in only the RPM model. Even in this case, only 80% and 64% of the η_1 and η_2 parameters were comparable to previoulsy reported values, respectively.

Estimation of the BCG wave features was the most accurate in the FPM with an average RMSE error of 0.018N in the I wave amplitude and 0.014N in the J wave

and 0.020N in the K wave. Results of the RPM showed RMSE values of 0.021N, 0.023N, and 0.031N for the I/J/K amplitudes. Timing of these waves was also the most accurate in the FPM model. Average RMSE values for the I, J and K waves times was 5.2ms, 5.7ms, and 6.5ms respectively. For the RPM, average RMSE values were higher at 6.4ms, 8.7ms, and 10.9ms for the I/J/K wave times.

Shortcomings of these model-based variants were identified, namely the inaccuracy of intermediate pressures and reflection coefficient parameters. Methods for improving these estimations were proposed as future work beyond this thesis.

Overall these models were able to provide comparably accurate PTT estimation by the BCG for the elucidation of ubiquitous BP monitoring. With this improved estimation method of PTT, the development of a ubiquitous BP monitoring device has been greatly facilitated. A previously presented mechanism model of the BCG was validated through this work. Further development of this BCG-based PTT model is expected to result in a greater understanding of patient-specific cardiovascular parameters and make the dream of truly ubiquitous BP monitoring a reality.

Appendix A: Equation Derivations

A.1 Transmission Line Theory

Provided below is the derivation of Equation 4.1. Figure A.1 illustrates the location of each pressure in the arterial tube. P_0 denotes the proximal pressure, whereas P_1 denotes the distal pressure and $\tau s = \gamma L$ (γ is the wave propagation coefficient).

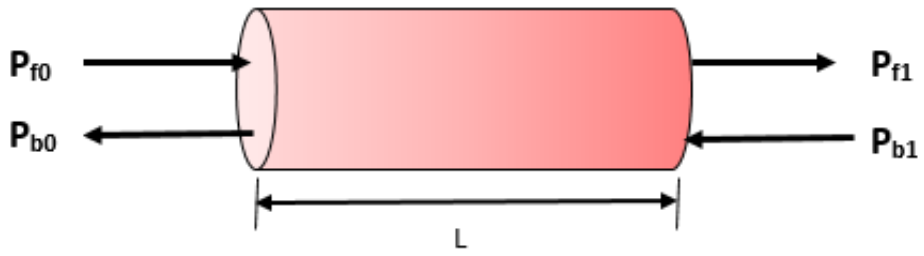

Figure A.1: Transmission Line Theory Pressures

The forward wave at the distal location, P_{f1} is simply the time-delay of the forward wave from the proximal location P_{f0}. The distal backward wave, P_{b1} is the forward wave at that site times the reflection coefficient, Γ. Finally, the backward wave at the proximal site P_{b0}, is the time-delay of the backward wave at the distal

site.

$$P_{f1} = e^{-\tau s} P_{f0} \tag{A.1}$$

$$P_{b1} = \Gamma(s) P_{f1} \tag{A.2}$$

$$P_{b0} = e^{-\tau s} P_{b1} \tag{A.3}$$

Since P_0 is the sum of its forward and backward waves, it can be written in the follow manner:

$$\begin{aligned} P_0 &= P_{f0} + P_{b0} \\ &= P_{f0}(1 + e^{-2\tau s}\Gamma(s)) \end{aligned} \tag{A.4}$$

Repeating for P_1:

$$\begin{aligned} P_1 &= P_{f1} + P_{b1} \\ &= P_{f0} e^{-\tau s}(1 + \Gamma(s)) \end{aligned} \tag{A.5}$$

Thus the relationship between the proximal and distal pressure is as follows:

$$\begin{aligned} \frac{P_0}{P_1} &= \frac{P_{f0}(1 + e^{-2\tau s}\Gamma(s))}{P_{f0} e^{-\tau s}(1 + \Gamma(s))} \\ \frac{P_0}{P_1} &= \frac{e^{\tau s} + e^{-\tau s}\Gamma(s)}{1 + \Gamma(s)} \\ P_0 &= \frac{e^{\tau s} + e^{-\tau s}\Gamma(s)}{1 + \Gamma(s)} P_1 \end{aligned} \tag{A.6}$$

A.2 Discretization of FPM and RPM Variants

The following chapter shall provide the explicit discretization of the RPM and FPM models from Equations 4.11 and 4.13 respectively.

A.2.1 FPM

Starting with Equation 4.13, the transformation from the Laplace domain to the time domain can be accomplished with the Z-transform where $s \approx F_s(z-1)$. We also approximate the time delays, τ_i, by setting equal to the discrete variable $\frac{n_i}{F_s}$.

$$\begin{aligned} BCG(s) &= \Bigg(- A_A \frac{e^{(\tau_1+\tau_2+\tau_3)s}(s+\eta_1) + e^{(\tau_3-\tau_1-\tau_2)s}\eta_2}{s+\eta_1+\eta_2} \\ &+ (A_A + A_D)\frac{e^{(\tau_2+\tau_3)s}(s+\eta_1) + e^{(\tau_3-\tau_2)s}\eta_2}{s+\eta_1+\eta_2} - A_D e^{\tau_3 s}\Bigg) P_3(s) \quad \text{(A.7)} \\ \Rightarrow BCG(k) &= \Bigg(- A_A \frac{e^{(n_1+n_2+n_3)(z-1)}(F_s(z-1)+\eta_1) + e^{(n_3-n_1-n_2)(z-1)}\eta_2}{F_s(z-1)+\eta_1+\eta_2} \\ &+ (A_A + A_D)\frac{e^{(n_2+n_3)(z-1)}(F_s(z-1)+\eta_1) + e^{(n_3-n_2)(z-1)}\eta_2}{F_s(z-1)+\eta_1+\eta_2} \quad \text{(A.8)} \\ &- A_D e^{n_3(z-1)}\Bigg) P_3(k) \end{aligned}$$

Rearranging, the relationship between BCG and P_3 becomes:

$$\begin{aligned} BCG(k)(z-1+\frac{\eta_1+\eta_2}{F_s}) &= \Bigg(- A_A(e^{(n_1+n_2+n_3)(z-1)}(z-1+\frac{\eta_1}{F_s}) \\ &+ \frac{\eta_2}{F_s}e^{(n_3-n_1-n_2)(z-1)} \\ &+ (A_A+A_D)(e^{(n_2+n_3)(z-1)}(z-1+\frac{\eta_1}{F_s}) \\ &+ \frac{\eta_2}{F_s}e^{(n_3-n_2)(z-1)}) \\ &- A_D(z-1+\frac{\eta_1+\eta_2}{F_s})e^{n_3(z-1)}\Bigg)P_3(k) \end{aligned} \tag{A.9}$$

Completing the discretization, the last transformation by z-transform properties can be made.

$$\begin{aligned} BCG[k+1] &= \Big(1-\frac{\eta_1+\eta_2}{F_s}\Big)BCG[k] - A_AP_3[k+n_1+n_2+n_3+1] \\ &+ A_A\Big(1-\frac{\eta_1}{F_s}\Big)P_3[k+n_1+n_2+n_3] - A_A(\Big(\frac{\eta_2}{F_s}\Big)P_3[k-n_1-n_2+n_3] \\ &+ (A_A+A_D)P_3[k+n_2+n_3+1] + (A_A+A_D)\Big(\frac{\eta_1}{Fs}-1\Big)P_3[k+n_2+n_3] \\ &+ (A_A+A_D)(\frac{\eta_2}{F_s})P_3[k-n_2+n_3] - A_DP_3[k+n_3+1] \\ &+ A_D\Big(1-\frac{\eta_1+\eta_2}{F_s}\Big)P_3[k+n_3] \end{aligned} \tag{A.10}$$

A.2.2 RPM

Repeating the procedure from the FPM section, the z-transform is applied to Equation 4.11:

$$\begin{aligned} BCG(s) &= \Bigg(- A_A \frac{e^{(\tau_1+\tau_2)s}(s+\eta_1) + e^{-(\tau_1+\tau_2)s}\eta_2}{s+\eta_1+\eta_2} \\ &+ (A_A + A_D)\frac{e^{\tau_2 s}(s+\eta_1) + e^{-\tau_2 s}\eta_2}{s+\eta_1+\eta_2} - A_D \Bigg) P_2(s) \\ \Rightarrow BCG(k) &= \Bigg(- A_A \frac{e^{(n_1+n_2)(z-1)}(F_s(z-1)+\eta_1) + e^{-(n_1+n_2)(z-1)}\eta_2}{F_s(z-1)+\eta_1+\eta_2} \\ &+ (A_A + A_D)\frac{e^{n_2(z-1)}(F_s(z-1)+\eta_1) + e^{-n_2(z-1)}\eta_2}{F_s(z-1)+\eta_1+\eta_2} \\ &- A_D \Bigg) P_2(k) \end{aligned} \tag{A.11}$$

Rearranging, the relationship between BCG and P_2 becomes:

$$\begin{aligned} BCG(k)(z-1+\frac{\eta_1+\eta_2}{F_s}) &= \Bigg(- A_A(e^{(n_1+n_2)(z-1)}(z-1+\frac{\eta_1}{F_s}) && \text{(A.12)} \\ &+ \frac{\eta_2}{F_s}e^{-(n_1+n_2)(z-1)}) \\ &+ (A_A + A_D)(e^{n_2(z-1)}(z-1+\frac{\eta_1}{F_s}) && \text{(A.13)} \\ &+ \frac{\eta_2}{F_s}e^{-n_2(z-1)}) \\ &- A_D(z-1+\frac{\eta_1+\eta_2}{F_s}) \Bigg) P_2(k) \end{aligned}$$

Completing the discretization, the last transformation by z-transform properties can be made.

$$
\begin{aligned}
BCG[k+1] &= \Big(1-\frac{\eta_1+\eta_2}{F_s}\Big)BCG[k] - A_A P_2[k+n_1+n_2+1] \\
&+ A_A\Big(1-\frac{\eta_1}{F_s}\Big)P_2[k+n_1+n_2] - A_A(\Big(\frac{\eta_2}{F_s}\Big)P_2[k-n_1-n_2] \\
&+ (A_A+A_D)P_2[k+n_2+1] + (A_A+A_D)\Big(\frac{\eta_1}{Fs}-1\Big)P_2[k+n_2] \\
&+ (A_A+A_D)(\frac{\eta_2}{F_s})P_2[k-n_2] - A_D P_2[k+1] \qquad \text{(A.14)} \\
&+ A_D\Big(1-\frac{\eta_1+\eta_2}{F_s}\Big)P_2[k]
\end{aligned}
$$

Bibliography

[1] Chang-Sei Kim, Stephanie L Ober, M Sean McMurtry, et al. Ballistocardiogram: Mechanism and potential for unobtrusive cardiovascular health monitoring. *Scientific Reports*, 6, 2016.

[2] Heart disease facts. https://www.cdc.gov/heartdisease/facts.htm. Web. 2015-08-10. Accessed: 2017-03-24.

[3] Dariush Mozaffarian, Emelia J Benjamin, Alan S Go, et al. Heart disease and stroke statistics2016 update. *Circulation*, 133(4):e38–e360, 2016.

[4] Kathleen R Dobbin. Noninvasive blood pressure monitoring. *Critical care nurse*, 22(2):123–124, 2002.

[5] Ramakrishna Mukkamala, Jin-Oh Hahn, Omer T Inan, et al. Toward ubiquitous blood pressure monitoring via pulse transit time: Theory and practice. *IEEE Transactions on Biomedical Engineering*, 62(8):1879–1901, 2015.

[6] Heiko Gesche, Detlef Grosskurth, Gert Küchler, and Andreas Patzak. Continuous blood pressure measurement by using the pulse transit time: Comparison to a cuff-based method. *European Journal of Applied Physiology*, 112(1):309–315, 2012.

[7] In cheol Jeong, Jeffrey Wood, and Joseph Finkelstein. Using individualized pulse transit time calibration to monitor blood pressure during exercise. *Informatics, Management and Technology in Healthcare*, 190:39, 2013.

[8] Michela Masè, Walter Mattei, Roberta Cucino, Luca Faes, and Giandomenico Nollo. Feasibility of cuff-free measurement of systolic and diastolic arterial blood pressure. *Journal of Electrocardiology*, 44(2):201–207, 2011.

[9] Heather Ting Ma. A blood pressure monitoring method for stroke management. *BioMed Research International*, 2014, 2014.

[10] BM McCarthy, CJ Vaughan, B O'flynn, A Mathewson, and C Ó Mathúna. An examination of calibration intervals required for accurately tracking blood pressure using pulse transit time algorithms. *Journal of Human Hypertension*, 27(12):744–750, 2013.

[11] Guanqun Zhang, Mingwu Gao, Da Xu, N Bari Olivier, and Ramakrishna Mukkamala. Pulse arrival time is not an adequate surrogate for pulse transit time as a marker of blood pressure. *Journal of Applied Physiology*, 111(6):1681–1686, 2011.

[12] Mingwu Gao, Hao-Min Cheng, Shih-Hsien Sung, et al. Estimation of pulse transit time as a function of blood pressure using a nonlinear arterial tube-load model. *IEEE Transactions on Biomedical Engineering*, 2016.

[13] Robert C Talley, Jerry F Meyer, and John L McNay. Evaluation of the preejection period as an estimate of myocardial contractility in dogs. *The American Journal of Cardiology*, 27(4):384–391, 1971.

[14] Willard S Harris, Clyde D Schoenfeld, and Arnold M Weissler. Effects of adrenergic receptor activation and blockade on the systolic preejection period, heart rate, and arterial pressure in man. *Journal of Clinical Investigation*, 46(11):1704, 1967.

[15] Zhihao Chen, Xiufeng Yang, Ju Teng Teo, and Soon Huat Ng. Noninvasive monitoring of blood pressure using optical ballistocardiography and photoplethysmograph approaches. In *Engineering in Medicine and Biology Society (EMBC), 2013 35th Annual International Conference of the IEEE*, pages 2425–2428. IEEE, 2013.

[16] Chang-Sei Kim, Andrew M Carek, Ramakrishna Mukkamala, Omer T Inan, and Jin-Oh Hahn. Ballistocardiogram as proximal timing reference for pulse transit time measurement: Potential for cuffless blood pressure monitoring. *IEEE Transactions on Biomedical Engineering*, 62(11):2657–2664, 2015.

[17] JW Gordon. Certain molar movements of the human body produced by the circulation of the blood. *Journal of Anatomy and Physiology*, 11(Pt 3):533, 1877.

[18] Isaac Starr. The relation of the bcg to cardiac function. *Am J Cardiol*, 2:737–747, 1958.

[19] Oscar Tannenbaum, Jerome A Schack, and Harry Vesell. Relationship between ballistocardiographic forces and certain events in the cardiac cycle. *Circulation*, 6(4):586–592, 1952.

[20] Isaac Starr, AJ Rawson, HA Schroeder, and NR Joseph. Studies on the estimation of cardiac ouptut in man, and of abnormalities in cardiac function, from the heart's recoil and the blood's impacts; the ballistocardiogram. *American Journal of Physiology–Legacy Content*, 127(1):1–28, 1939.

[21] JL Nickerson, J Vr Warren, and ES Brannon. The cardiac output in man: Studies with the low frequency, critically-damped ballistocardiograph, and the method of right atrial catheterization. *Journal of Clinical Investigation*, 26(1):1, 1947.

[22] WR Scarborough. Current status of ballistocardiography. *Progress in Cardiovascular Diseases*, 2(3):263–291, 1959.

[23] Michael Tobin, John N Edson, Robert Dickes, Gerald H Flamm, and Lawrence Deutsch. The elimination of body resonance distortion from the direct-body ballistocardiogram. *Circulation*, 12(1):108–113, 1955.

[24] TJ Reeves, H Ellison, EE Eddleman, and Andrew F Spear. The application of direct body ballistocardiography to force ballistocardiography. *The Journal of Laboratory and Clinical Medicine*, 49(4):545–560, 1957.

[25] Isaac Starr and Abraham Noordergraaf. A comparison between ultralow-frequency ballistocardiograms and those secured by an improved high-frequency technique, with studies to explain remaining differences. *American Heart Journal*, 64(1):79–100, 1962.

[26] Maurice B Rappaport. Displacement, velocity, and acceleration ballistocardiograms as registered with an undamped bed of ultralow natural frequency: Ii. instrumental considerations. *American Heart Journal*, 52(5):643–652, 1956.

[27] TJ Reeves, WB Jones, and LL Hefner. Design of an ultra low frequency force ballistocardiograph on the principle of the horizontal pendulum. *Circulation*, 16(1):36–42, 1957.

[28] John L Nickerson and Howard J Curtis. The design of the ballistocardiograph. *American Journal of Physiology–Legacy Content*, 142(1):1–11, 1944.

[29] Wm R Scarborough, jr FW Davis, BM Baker, RE Mason, and ML Singewald. A review of ballistocardiography. *American Heart Journal*, 44(6):910–946, 1952.

[30] RS Guber, M Rodstein, and HE Ungerleider. Ballistocardiograph: An appraisal of technic, physiological principles, and clinic value. *Circulation*, 7:268–286, 1953.

[31] Piney Pollock. Ballistocardiography: A clinical review. *Canadian Medical Association Journal*, 76(9):778, 1957.

[32] William R Scarborough, Edgar F Folk, Patricia M Smith, and Joseph H Condon. The nature of records from ultra-low frequency ballistocardiographic systems and their relation to circulatory events. *The American Journal of Cardiology*, 2(5):613–641, 1958.

[33] JJ Wang and KH Parker. Wave propagation in a model of the arterial circulation. *Journal of Biomechanics*, 37(4):457–470, 2004.

[34] WF Hamilton, P Dow, and JW Remington. The relationship between the cardiac ejection curve and the ballistocardiographic forces. *American Journal of Physiology*, 144:557–570, 1945.

[35] Abraham Noordergraaf and Chris E Heynekamp. Genesis of displacement of the human longitudinal ballistocardiogram from the changing blood distribution. *The American Journal of Cardiology*, 2(6):748–756, 1958.

[36] Stephanie L-O Martin, Andrew M Carek, Chang-Sei Kim, et al. Weighing scale-based pulse transit time is a superior marker of blood pressure than conventional pulse arrival time. *Scientific Reports*, 6, 2016.

[37] Hazar Ashouri, Lara Orlandic, and Omer T Inan. Unobtrusive estimation of cardiac contractility and stroke volume changes using ballistocardiogram measurements on a high bandwidth force plate. *Sensors*, 16(6):787, 2016.

[38] JH Atterhög, KEITH Eliasson, and PAUL Hjemdahl. Sympathoadrenal and cardiovascular responses to mental stress, isometric handgrip, and cold pressor test in asymptomatic young men with primary t wave abnormalities in the electrocardiogram. *British Heart Journal*, 46(3):311, 1981.

[39] Sydney B Miller and Aurelio Sita. Parental history of hypertension, menstrual cycle phase, and cardiovascular response to stress. *Psychosomatic Medicine*, 56(1):61–69, 1994.

[40] Gonneke Willemsen, Christopher Ring, Douglas Carroll, et al. Secretory immunoglobulin a and cardiovascular reactions to mental arithmetic and cold pressor. *Psychophysiology*, 35(3):252–259, 1998.

[41] Elizabeth Sibolboro Mezzacappa, Robert M Kelsey, Edward S Katkin, and Richard P Sloan. Vagal rebound and recovery from psychological stress. *Psychosomatic Medicine*, 63(4):650–657, 2001.

[42] Robert M Kelsey, Sidney R Ornduff, and Bruce S Alpert. Reliability of cardiovascular reactivity to stress: Internal consistency. *Psychophysiology*, 44(2):216–225, 2007.

[43] RA Payne, CN Symeonides, DJ Webb, and SRJ Maxwell. Pulse transit time measured from the ecg: An unreliable marker of beat-to-beat blood pressure. *Journal of Applied Physiology*, 100(1):136–141, 2006.

[44] Edgar A Hines and George E Brown. The cold pressor test for measuring the reactibility of the blood pressure: Data concerning 571 normal and hypertensive subjects. *American Heart Journal*, 11(1):1–9, 1936.

[45] Guanqun Zhang, Jin-Oh Hahn, and Ramakrishna Mukkamala. Tube-load model parameter estimation for monitoring arterial hemodynamics. *Engineering Approaches to Study Cardiovascular Physiology: Modeling, Estimation, and Signal Processing*, page 20, 2011.

[46] AP Avolio. Multi-branched model of the human arterial system. *Medical and Biological Engineering and Computing*, 18(6):709–718, 1980.

[47] Majid Abdollahzade, Chang-Sei Kim, Nima Fazeli, et al. Data-driven lossy tube-load modeling of arterial tree: In-human study. *Journal of Biomechanical Engineering*, 136(10):101011, 2014.

[48] MUSTAFA Karamanoglu and MICHAEL P Feneley. Derivation of the ascending aortic-carotid pressure transfer function with an arterial model. *American Journal of Physiology-Heart and Circulatory Physiology*, 271(6):H2399–H2404, 1996.

[49] Masaru Sugimachi, Toshiaki Shishido, Kunio Miyatake, and Kenji Sunagawa. A new model-based method of reconstructing central aortic pressure from peripheral arterial pressure. *The Japanese Journal of Physiology*, 51(2):217–222, 2001.

[50] Gokul Swamy, Da Xu, N Bari Olivier, and Ramakrishna Mukkamala. An adaptive transfer function for deriving the aortic pressure waveform from a peripheral artery pressure waveform. *American Journal of Physiology-Heart and Circulatory Physiology*, 297(5):H1956–H1963, 2009.

[51] Jin-Oh Hahn, Andrew T Reisner, Farouc A Jaffer, and H Harry Asada. Subject-specific estimation of central aortic blood pressure using an individualized transfer function: A preliminary feasibility study. *IEEE Transactions on Information Technology in Biomedicine*, 16(2):212–220, 2012.

[52] Jin-Oh Hahn. Individualized estimation of the central aortic blood pressure waveform: A comparative study. *IEEE Journal of Biomedical and Health Informatics*, 18(1):215–221, 2014.

[53] ROBERTO Burattini and KENNETH B Campbell. Effective distributed compliance of the canine descending aorta estimated by modified t-tube model. *American Journal of Physiology-Heart and Circulatory Physiology*, 264(6):H1977–H1987, 1993.

[54] Da Xu, Guanqun Zhang, N Bari Olivier, and Ramakrishna Mukkamala. Monitoring aortic stiffness in the presence of measurement artifact based on an arterial tube model. In *Engineering in Medicine and Biology Society (EMBC), 2010 Annual International Conference of the IEEE*, pages 3453–3456. IEEE, 2010.

[55] Guanqun Zhang, Mingwu Gao, and Ramakrishna Mukkamala. Robust, beat-to-beat estimation of the true pulse transit time from central and peripheral blood pressure or flow waveforms using an arterial tube-load model. In *Engineering in Medicine and Biology Society, EMBC, 2011 Annual International Conference of the IEEE*, pages 4291–4294. IEEE, 2011.

[56] Mustafa Karamanoglu, David E Gallagher, Albert P Avolio, and Michael F O'Rourke. Pressure wave propagation in a multibranched model of the human

upper limb. *American Journal of Physiology-Heart and Circulatory Physiology*, 269(4):H1363–H1369, 1995.

[57] Mohammad Rashedi, Nima Fazeli, Alyssa Chappell, et al. Comparative study on tube-load modeling of arterial hemodynamics in humans. *Journal of Biomechanical Engineering*, 135(3):031005, 2013.